

TIME-VARIABLE COMPLEX METAL ABSORPTION LINES IN THE QUASAR HS 1603+3820¹

TORU MISAWA,² MICHAEL ERACLEOUS,² JANE C. CHARLTON,² AND AKITO TAJITSU³

Received 2004 October 18; accepted 2005 April 26

ABSTRACT

We present a new spectrum of the quasar HS 1603+3820 taken 1.28 yr (0.36 yr in the quasar rest frame) after a previous observation with Subaru+HDS. The new spectrum enables us to search for time variability as an identifier of intrinsic narrow absorption lines (NALs). This quasar shows a rich complex of C IV NALs within 60,000 km s⁻¹ of the emission redshift. On the basis of covering factor analysis, Misawa et al. found that the C IV NAL system at $z_{\text{abs}} = 2.42\text{--}2.45$ (system A, at a shift velocity of $v_{\text{sh}} = 8300\text{--}10,600$ km s⁻¹ relative to the quasar) was intrinsic to the quasar. With our new spectrum, we perform time variability analysis, as well as covering factor analysis, to separate intrinsic NALs from intervening NALs for eight C IV systems. Only system A, which was identified as an intrinsic system in the earlier paper by Misawa et al., shows a strong variation in line strength ($W_{\text{obs}} \approx 10.4 \rightarrow 19.1$ Å). We speculate that a broad absorption line (BAL) could be forming in this quasar (i.e., many narrower lines will blend together to make a BAL profile). We illustrate the plausibility of this suggestion with the help of a simulation in which we vary the column densities and covering factors of the NAL complex. Under the assumption that a change of ionization state causes the variability, a lower limit can be placed on the electron density ($n_e \gtrsim 3 \times 10^4$ cm⁻³) and an upper limit on the distance from the continuum source ($r \leq 6$ kpc). On the other hand, if the motion of clumpy gas causes the variability (a more likely scenario), the crossing velocity and the distance from the continuum source are estimated to be $v_{\text{cross}} > 8000$ km s⁻¹ and $r < 3$ pc. In this case, the absorber does not intercept any flux from the broad emission line region, but only flux from the UV continuum source. If we adopt the dynamical model of Murray et al., we can obtain a much more strict constraint on the distance of the gas parcel from the continuum source, $r < 0.2$ pc.

Subject headings: quasars: absorption lines — quasars: individual (HS 1603+3820)

1. INTRODUCTION

QSO absorption lines are usually classified by the width of their profiles: broad absorption lines (BALs; FWHM > 2000 km s⁻¹), narrow absorption lines (NALs; FWHM $< 200\text{--}300$ km s⁻¹), and mini-BALs (intermediate class between BALs and NALs; Hamann & Sabra 2004). Because of their large blueshifts and their wide and smooth line profiles, BALs are plausibly associated with accretion disk winds (e.g., Murray & Chiang 1995; Arav et al. 1995; Proga et al. 2000). But BALs appear in only $\sim 10\%$ of optically selected quasars (Weymann et al. 1991).

On the other hand, NALs can arise from both intervening absorbers (e.g., cosmologically intervening galaxies, intergalactic medium, and quasar host galaxies) and intrinsic absorbers (i.e., clouds that are physically associated with the quasars). A significant fraction of NALs are thought to be intrinsic to the quasars and may arise in gas that is outflowing from the central region, based on a statistical analysis (Richards et al. 1999; Richards 2001). In the spectra of radio-quiet and flat radio spectrum quasars, intrinsic NALs can appear at large shift velocities of up to 30,000 km s⁻¹ (Richards et al. 1999). Because NALs are often not saturated, they provide a powerful diagnostic of the physical conditions of the gas clouds that are physically associated with the quasars.

In order to understand the quasar central region using NALs, we must determine which ones are intrinsic to the quasars. We can use several criteria to separate intrinsic NALs from intervening NALs, e.g., time variability, high electron density, partial

coverage, polarization, line profile, high ionization state, and high metallicity (Barlow & Sargent 1997; Hamann et al. 1997b and references therein). Among them, two methods, (1) time variability analysis and (2) covering factor analysis, are the most reliable and most frequently applied (e.g., Barlow et al. 1992; Hamann et al. 1997a, 1997b; Barlow & Sargent 1997; Goodrich & Miller 1995; Ganguly et al. 1999, 2003; Misawa et al. 2003; Narayanan et al. 2004; Wise et al. 2004).

In this paper, we apply the above tests to the absorption lines of the bright quasar HS 1603+3820 ($z_{\text{em}} = 2.542$, $B = 15.9$). First discovered in the Hamburg/CfA Bright Quasar Survey (Hagen et al. 1995; Dobrzycki et al. 1996), this quasar shows a large number of metal NALs in the vicinity of the emission redshift. Dobrzycki et al. (1999; hereafter D99) detected 13 C IV NALs at $1.965 < z_{\text{abs}} < 2.554$ in their intermediate-resolution spectrum ($R \sim 3000$). The number density of C IV Poisson systems⁴ with rest-frame equivalent width $W_{\text{rest}} > 0.15$ Å is $dN/dz \sim 12$ at $z_{\text{abs}} \sim 2.38$ in the spectrum of HS 1603+3820 (Misawa et al. 2003, hereafter M03), while the global average value is $dN/dz = 2.5_{-0.5}^{+0.6}$ at $z_{\text{abs}} = 2.40$ (Sargent et al. 1988; Steidel 1990; Misawa et al. 2002). Even though the same trends have already been noted statistically for the class of radio-loud quasars (Foltz et al. 1986), such an extreme clustering is significant and probably related to the environment around the quasar (e.g., intrinsic material, a cluster of galaxies around the quasar, or a proximity effect due to the UV flux from the quasar).

M03 presented a high-resolution ($R \sim 45,000$) spectrum of the quasar that covered nine of the 13 C IV NALs at $z_{\text{abs}} > 2.29$, although one of them was apparently not real, since it was not detected in that higher quality spectrum. Using only covering factor

¹ Based on data collected at the Subaru Telescope, which is operated by the National Astronomical Observatory of Japan.

² Department of Astronomy and Astrophysics, Pennsylvania State University, 525 Davey Lab, University Park, PA 16802; misawa@astro.psu.edu, mce@astro.psu.edu, charlton@astro.psu.edu.

³ Subaru Telescope, National Astronomical Observatory of Japan, Hilo, HI 96720; tajitsu@naoj.org.

⁴ Groups of C IV NALs that lie within 1000 km s⁻¹ of each other are classified as a Poisson system because these could be produced in the same physical structure (e.g., Sargent et al. 1988; Steidel 1990; Misawa et al. 2002).

analysis, they concluded that the C IV NALs at $2.42 < z_{\text{abs}} < 2.45$ (system A in M03) are intrinsic to the quasar, at velocity shifts⁵ from the quasar $v_{\text{sh}} = 8300\text{--}10,600 \text{ km s}^{-1}$. On the other hand, systems B, C, and D at $z_{\text{abs}} = 2.48\text{--}2.55$ could not be demonstrated to be intrinsic, although systems C and D are close (within 1000 km s^{-1}) to the quasar emission redshift. In fact, one of them (system D) is redshifted from the quasar. These absorbers (especially the redshifted system) could still be intrinsic, but with clouds that happened to cover the emission source entirely at the time of observation. Partial coverage is a sufficient but not a necessary condition to demonstrate the intrinsic nature of an absorber.

In this paper, we present a new spectrum of the quasar taken with the same instrument configuration as our previous spectrum, 1.28 yr after the previous observation (0.36 yr in the quasar rest frame) with the High Dispersion Spectrograph (HDS; Noguchi et al. 2002) on the Subaru Telescope. Our additional spectrum enables us to search for time variability of absorption lines as an identifier of intrinsic NALs, which will not only strengthen our classification results but also constrain several parameters of the intrinsic NAL absorbers.

In § 2, we describe the observations and data reduction. The methods of line identification and line classification are outlined in §§ 3 and 4. In § 5, the properties of eight C IV systems, including four new systems, are examined in detail, and the possible origins of the time variability are discussed in § 6. We summarize our results in § 7. In this paper, we use a cosmology with $H_0 = 72 \text{ km s}^{-1} \text{ Mpc}^{-1}$, $\Omega_m = 0.3$, and $\Omega_\Lambda = 0.7$.

2. OBSERVATION AND DATA REDUCTION

We obtained a spectrum of HS 1603+3820 with Subaru+HDS on 2003 July 7 (UT). We adopt $z_{\text{em}} = 2.542$ as the systemic redshift of the quasar, which was estimated by matching the spectrum of D99 to the Sloan Digital Sky Survey composite spectrum by using the O I $\lambda 1304$, Si II $\lambda 1307$, and C II $\lambda 1335$ emission lines (M03). We used a $0''.8$ slit width ($R \sim 45,000$) and adopted 2 pixel binning along the slit. The red grating with a central wavelength of 4900 \AA was chosen, which covers the range $3530\text{--}4800 \text{ \AA}$ on the blue CCD and $4980\text{--}6180 \text{ \AA}$ on the red CCD. This configuration covers all C IV NALs identified in D99. We took three spectra with exposure times of 3600, 3600, and 2400 s, respectively. Since the weather conditions were not good at the beginning of the observation, we used only the last two exposures to produce the final spectrum. We reduced the data in a standard manner with the IRAF software.⁶ Wavelength calibration was carried out using the spectrum of a Th-Ar lamp. Because the blaze profile function of each echelle order is changing with time, we cannot perform flux calibration using the spectrum of a standard star. Therefore, we directly fitted the continuum, which also includes substantial contributions from broad emission lines, with a third-order cubic spline function. Around heavily absorbed regions, in which direct continuum fitting is difficult, we use the interpolation technique introduced in M03. We have already confirmed the validity of this technique by applying it to a stellar spectrum in M03; the continuum model is good to 3.3% or better. After binning every 3 pixels, the signal-to-noise ratio (S/N) in our 6000 s exposure is ~ 70 per resolution element around $\lambda = 5450 \text{ \AA}$. In Figure 1, we show the normalized spectrum of the region redward of the Ly α emission line of the quasar. Echelle

order gaps and bad pixels in the detector cause the defects seen in the spectrum. The spectrum in the region of the Ly α forest is not presented because of low reliability of continuum fitting, although some strong metal lines were identified by fitting the continuum locally.

3. LINE DETECTION AND FITTING

For the present work, we used the line-fitting software package MINFIT (Churchill 1997; Churchill et al. 2003), while we used VPFIT (Webb 1987; Carswell et al. 1987) in M03. The MINFIT code can fit absorption profiles using not only redshift (z), column density ($\log N$ in cm^{-2}), and Doppler parameter (b) but also covering factor (C_f , described below) as a free parameter.

D99 detected 13 C IV NALs at $1.88 < z_{\text{abs}} < 2.55$ in their intermediate-resolution spectrum. In our new spectrum, we identified 11 of the 13 C IV NALs in that range. We also found a new C IV NAL at $z_{\text{abs}} = 2.2653$. We did *not* detect two C IV NALs found in D99, at $z_{\text{abs}} = 2.1762$ and 2.5114 ; the former is unfortunately in the echelle order gap in our new spectrum, and the latter seems to be a false detection because it was noted as uncertain in D99 and it is not detected in either the spectrum of M03 (hereafter first spectrum) or the spectrum of this paper (hereafter second spectrum). In total, 12 C IV NALs were detected in our new spectrum.

Following the method of M03, we divided these C IV NALs into eight systems (systems A–H in Fig. 1). System A contains five C IV NALs, while the other systems have only one NAL, as identified in D99. These NALs are resolved into multiple components in our high-resolution spectrum (we refer to these as “doublets” in the case of the C IV, N V, and Si IV lines and “lines” for other single metal lines). The first four systems (systems A–D) had already been identified in M03. An additional four systems, at $z_{\text{abs}} = 1.88\text{--}2.26$ (systems E–H), are blueshifted from the other systems and were not covered by the first spectrum. After careful fitting trials with MINFIT, we found 47 C IV, 14 Si IV, and six N V doublets and 54 other single metal lines associated with the eight C IV systems. We also fitted four systems in the first spectrum again, using MINFIT, and confirmed that the results with VPFIT in M03 are consistent with the results of MINFIT.

The fit parameters of these systems are summarized in Table 1 for NALs already identified in the first spectrum and in Table 2 for NALs detected in only the second spectrum. Column (1) is the metal line identification (ID) number. Columns (2) and (3) give the observed wavelength and redshift. Column (4) gives the velocity shift from the quasar systemic redshift, and column (5), the Doppler parameter. Columns (6) and (7) give the covering factors and column densities with 1σ Poisson error bars (see discussion in § 4.1). Columns (2)–(7) in Table 1 are the parameters of the components detected in the first spectrum. The corresponding parameters for the second spectrum are presented in columns (8)–(13). The same parameters for newly identified NALs are listed in Table 2. Results of a fit for the C IV doublets in system A, carried out manually (as described in § 4.1), are given in Table 1. Manual fitting was necessary because these doublets are so heavily blended with each other and with other lines that line fitting with MINFIT could not be applied. For the same reason, the fit parameters for the Si II $\lambda 1526$ lines in system B are evaluated in the same manner, with fitting errors evaluated with the help of the χ^2 test. For all other doublets, C_f is a free parameter.

4. IDENTIFICATION OF INTRINSIC NALs

Here we describe two methods of determining that a given NAL is intrinsic: (1) covering factor analysis and (2) time variability analysis.

⁵ The shift velocity is defined as positive for NALs that are blueshifted from the quasar, which is opposite to the definition given in M03.

⁶ IRAF is distributed by the National Optical Astronomy Observatory, which is operated by the Association of Universities for Research in Astronomy, Inc., under cooperative agreement with the National Science Foundation.

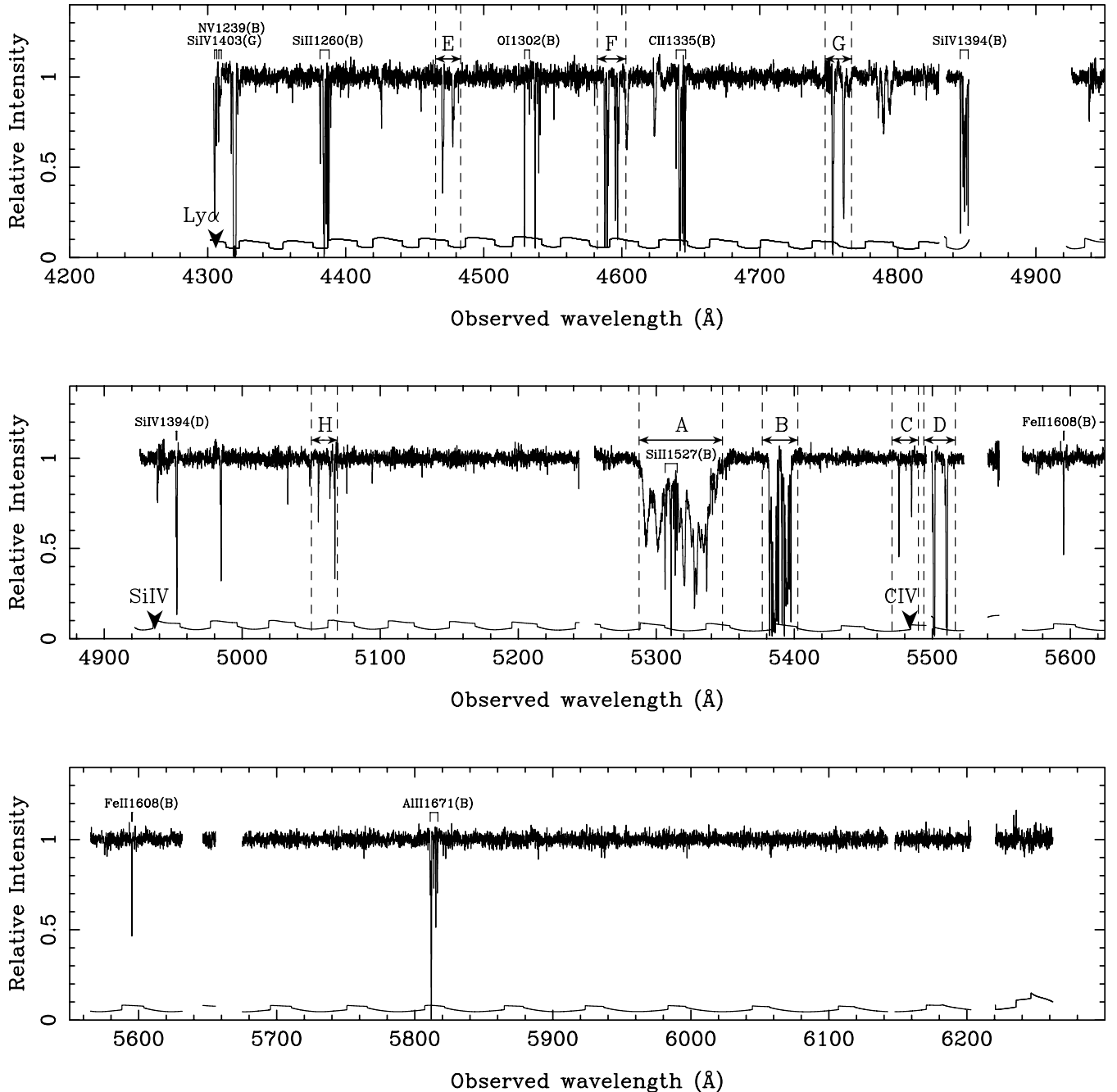


FIG. 1.—Normalized spectrum of HS 1603+3820 (binned by 3 pixels) showing the C IV absorption systems, as well as other metal lines. The quasar emission lines of Ly α , Si IV λ 1394, and C IV λ 1548 are marked with downward arrows. The region blueward of the Ly α emission line is not shown because the spectrum normalization by continuum fitting is not reliable in the Ly α forest. The lower line is the 1σ error spectrum. The regions affected by either data defects or echelle order gaps are masked.

4.1. Covering Factor Analysis

The covering factor, C_f , is the line-of-sight coverage fraction of the absorber over the continuum source and the emission-line region. The effective covering factor is evaluated by considering the fraction of photons from the background source(s) intercepted by the absorbing gas. The normalized flux at wavelength λ is given by

$$R(\lambda) = [1 - C_f(\lambda)] + C_f(\lambda)e^{-\tau(\lambda)}, \quad (1)$$

where $\tau(\lambda)$ is the optical depth at λ . For a resonant doublet such as C IV $\lambda\lambda$ 1548, 1551, the ratio of the oscillator strengths of blue

and red members is 2, as dictated by atomic physics. Therefore, we can evaluate the covering factors as a function of velocity for doublets using the following equation:

$$C_f(v) = \frac{1 + R_r^2(v) - 2R_r(v)}{1 + R_b(v) - 2R_r(v)}, \quad (2)$$

where $R_b(v)$ and $R_r(v)$ are the residual fluxes of the blue and red members of the doublets in the normalized spectrum (Hamann et al. 1997b; Barlow & Sargent 1997; Crenshaw et al. 1999). In general, the emission-line region and continuum source could have different covering factors, as discussed by Ganguly et al. (1999).

TABLE 1
METAL LINES DETECTED IN FIRST AND SECOND SPECTRA

Line ID (1)	λ_{obs} (Å) (2)	z_{abs} (3)	V (km s ⁻¹) (4)	b (km s ⁻¹) (5)	C_f (6)	$\log N$ (cm ⁻²) (7)	λ_{obs} (Å) (8)	z_{abs} (9)	V (km s ⁻¹) (10)	b (km s ⁻¹) (11)	C_f (12)	$\log N$ (cm ⁻²) (13)
System A: $z_{\text{abs}} = 2.4302$												
C IV $\lambda 1548$:												
1.....	5292.6	2.4185	10646	86 ± 2^a	0.31 ± 0.01^a	14.59 ± 0.04^a	5292.6	2.4185	10639	88 ± 1^a	0.44 ± 0.01^a	14.62 ± 0.01^a
2.....							5298.4	2.4222	10319	406 ± 8^a	0.44^a	14.76 ± 0.01^a
3.....	5301.6	2.4246	10106	238 ± 5^a	0.31^a	14.59 ± 0.01^a						
4.....	5316.5	2.4340	9287	60.3^b	...	13.60^b	5316.8	2.4342	9269	70.7^b	...	13.91^b
5.....	5319.8	2.4361	9104	78.5^b	...	13.82^b	5319.9	2.4362	9095	77.7^b	...	14.20^b
6.....	5320.4	2.4365	9069	27.1^b	...	13.45^b	5320.5	2.4366	9060	23.2^b	...	13.36^b
7.....	5322.8	2.4381	8929	50.7^b	...	12.84^b	5322.8	2.4381	8929	48.1^b	...	13.53^b
8.....							5324.1	2.4389	8859	31.5^b	...	13.15^b
9.....	5326.1	2.4402	8746	289.3^b	...	13.97^b	5325.8	2.4400	8764	84.1^b	...	13.91^b
10.....	5327.6	2.4412	8659	9.9^b	...	13.23^b	5327.6	2.4412	8659	12.3^b	...	13.54^b
11.....	5327.6	2.4412	8659	42.1^b	...	13.47^b	5327.6	2.4412	8659	41.1^b	...	13.80^b
12.....	5329.4	2.4423	8563	38.9^b	...	13.29^b	5329.4	2.4423	8563	51.8^b	...	13.96^b
13.....							5330.7	2.4432	8485	24.1^b	...	12.94^b
14.....	5331.7	2.4438	8433	59.4^b	...	13.34^b	5331.8	2.4439	8424	49.0^b	...	13.70^b
15.....	5334.2	2.4454	8293	54.8^b	...	13.54^b	5334.3	2.4455	8285	82.1^b	...	13.99^b
System B: $z_{\text{abs}} = 2.4785$												
Al II $\lambda 1671$:												
1.....	5811.2	2.4781	5461	11.9 ± 0.8	...	11.99 ± 0.02	5811.3	2.4782	5452	10.6 ± 1.1	...	11.88 ± 0.04
2.....	5812.0	2.4786	5418	9.3 ± 0.2	...	12.88 ± 0.02	5812.0	2.4786	5418	9.3 ± 0.3	...	12.81 ± 0.03
3.....	5813.3	2.4794	5349	4.8 ± 1.6	...	11.23 ± 0.08	5813.3	2.4794	5349	1.3 ± 3.5	...	11.03 ± 0.14
4.....	5813.8	2.4797	5323	5.7 ± 0.6	...	11.75 ± 0.03	5813.8	2.4797	5323	4.8 ± 0.9	...	11.62 ± 0.05
5.....	5815.2	2.4805	5254	2.9 ± 0.3	...	11.95 ± 0.03	5815.2	2.4805	5254	2.8 ± 0.5	...	11.91 ± 0.04
6.....	5816.3	2.4812	5194	3.8 ± 0.7	...	11.71 ± 0.05	5816.3	2.4812	5194	3.1 ± 1.2	...	11.62 ± 0.10
7.....	5816.7	2.4814	5177	6.2 ± 1.6	...	11.55 ± 0.08	5816.5	2.4813	5185	5.7 ± 3.5	...	11.36 ± 0.19
C IV $\lambda 1548$:												
1.....	5381.8	2.4762	5627	8.5 ± 0.3^c	...	13.36 ± 0.01^c	5381.8	2.4762	5625	8.6 ± 0.6	1.54 ± 0.61	13.07 ± 0.21
2.....	5382.2	2.4764	5606	6.6 ± 0.2^c	...	14.08 ± 0.02^c	5382.1	2.4764	5608	7.3 ± 0.3	0.98 ± 0.02	14.06 ± 0.05
3.....	5382.8	2.4768	5571	23.2 ± 1.0^c	...	13.49 ± 0.02^c	5382.8	2.4768	5573	14.2 ± 2.0^c	...	13.31 ± 0.06^c
4.....	5383.0	2.4770	5559	2.2 ± 1.3^c	...	12.27 ± 0.09^c	5383.1	2.4770	5556	3.6 ± 2.1^c	...	12.51 ± 0.22^c
5.....							5383.4	2.4772	5539	9.7 ± 3.9^c	...	11.51 ± 9.99^c
6.....							5383.5	2.4773	5530	25.0 ± 2.0^c	...	13.27 ± 0.23^c
7.....	5383.8	2.4775	5517	16.5 ± 2.0	0.95 ± 0.03	13.67 ± 0.18	5383.8	2.4775	5513	9.0 ± 0.5	0.99 ± 0.02	14.22 ± 0.05
8.....	5383.9	2.4775	5511	7.2 ± 0.6^c	...	14.16 ± 0.04^c						
9.....	5384.5	2.4779	5477	14.9 ± 5.5	1.01 ± 0.15	13.59 ± 0.09	5384.5	2.4779	5478	12.5 ± 0.9	1.00 ± 0.07	13.72 ± 0.06
10.....	5384.5	2.4779	5475	4.1 ± 1.4	0.85 ± 0.56	13.10 ± 0.43						
11.....	5385.0	2.4783	5447	13.5 ± 1.4^c	...	14.03 ± 0.05^c	5385.1	2.4783	5444	12.4 ± 1.4	0.98 ± 0.03	14.02 ± 0.05
12.....	5385.4	2.4785	5428	5.0 ± 3.0	0.99 ± 0.47	13.09 ± 0.70	5385.6	2.4786	5418	12.9 ± 2.9	0.85 ± 0.08	14.00 ± 0.09
13.....	5385.6	2.4787	5413	12.8 ± 6.2	0.98 ± 0.01	13.99 ± 0.19						
14.....	5386.1	2.4790	5386	7.7 ± 1.7	0.89 ± 0.07	13.93 ± 0.06	5386.2	2.4790	5383	26.1 ± 2.1	0.99 ± 0.03	14.20 ± 0.06
15.....	5386.3	2.4791	5378	27.2 ± 0.5^c	...	13.90 ± 0.01^c						

TABLE 1—Continued

Line ID (1)	λ_{obs} (Å) (2)	z_{abs} (3)	V (km s ⁻¹) (4)	b (km s ⁻¹) (5)	C_f (6)	$\log N$ (cm ⁻²) (7)	λ_{obs} (Å) (8)	z_{abs} (9)	V (km s ⁻¹) (10)	b (km s ⁻¹) (11)	C_f (12)	$\log N$ (cm ⁻²) (13)
16.....	5387.1	2.4796	5334	6.2 ± 1.2	1.29 ± 1.50	12.73 ± 0.57	5387.3	2.4797	5323	16.4 ± 1.8	0.69 ± 0.29	13.68 ± 0.26
17.....	5387.4	2.4798	5317	8.2 ± 0.3	0.98 ± 0.02	13.75 ± 0.03	5387.4	2.4798	5314	7.0 ± 0.9	1.02 ± 0.19	13.49 ± 0.16
18.....	5388.4	2.4804	5262	18.2 ± 2.4	0.59 ± 0.77	13.25 ± 0.65	5388.3	2.4804	5263	11.3 ± 4.4	0.16 ± 0.02	14.05 ± 0.36
19.....	5388.6	2.4806	5250	4.7 ± 0.2	0.97 ± 0.02	13.97 ± 0.06	5388.6	2.4806	5246	4.7 ± 0.4	0.93 ± 0.03	14.06 ± 0.15
Fe II λ 1608:												
1.....	5595.1	2.4786	5418	4.1 ± 0.5	...	13.69 ± 0.03	5595.1	2.4786	5418	6.3 ± 0.5	...	13.60 ± 0.03
Si II λ 1527:												
1.....	5302.9	2.4737	5840	22.9 ± 4.8 ^c	...	13.06 ± 0.07 ^c	5302.9	2.4737	5840	19.0 ± 6.2 ^c	...	13.04 ± 0.06 ^c
2.....	5303.7	2.4742	5797	21.8 ± 3.1 ^c	...	13.14 ± 0.02 ^c	5303.7	2.4742	5797	23.7 ± 3.8 ^c	...	13.10 ± 0.07 ^c
3.....	5304.6	2.4748	5746	23.6 ± 4.8 ^c	...	12.95 ± 0.04 ^c	5304.6	2.4748	5746	19.1 ± 4.0 ^c	...	12.95 ± 0.08 ^c
4.....	5306.4	2.4757	5668	11.2 ± 0.1 ^c	...	13.63 ± 0.01 ^c	5306.4	2.4757	5668	10.9 ± 0.8 ^c	...	13.61 ± 0.03 ^c
5.....	5307.4	2.4765	5608	13.8 ± 0.8 ^c	...	13.04 ± 0.03 ^c	5307.6	2.4765	5599	12.3 ± 1.1 ^c	...	13.03 ± 0.06 ^c
6.....	5310.2	2.4782	5452	14.2 ± 1.0 ^c	...	13.24 ± 0.02 ^c	5310.0	2.4782	5461	14.2 ± 2.3 ^c	...	13.24 ± 0.06 ^c
7.....	5310.8	2.4786	5418	11.2 ± 0.1 ^c	...	14.07 ± 0.02 ^c	5310.8	2.4786	5418	11.2 ± 0.3 ^c	...	14.07 ± 0.03 ^c
8.....	5312.5	2.4798	5323	12.3 ± 0.4 ^c	...	13.17 ± 0.01 ^c	5312.5	2.4798	5323	12.3 ± 1.5 ^c	...	13.17 ± 0.02 ^c
9.....	5313.7	2.4805	5254	4.7 ± 0.2 ^c	...	13.45 ± 0.01 ^c	5313.9	2.4805	5246	5.6 ± 0.2 ^c	...	13.41 ± 0.03 ^c
10.....	5314.8	2.4812	5194	7.2 ± 0.5 ^c	...	13.22 ± 0.03 ^c	5314.8	2.4812	5194	7.8 ± 0.9 ^c	...	13.22 ± 0.05 ^c
11.....	5315.1	2.4815	5177	11.7 ± 0.4 ^c	...	13.43 ± 0.02 ^c	5315.2	2.4815	5168	11.5 ± 0.4 ^c	...	13.49 ± 0.02 ^c
System C: $z_{\text{abs}} = 2.5370$												
C IV λ 1548:												
1.....	5475.8	2.5369	432	11.6 ± 0.3	1.10 ± 0.17	13.30 ± 0.09	5475.8	2.5369	432	11.4 ± 0.5	0.88 ± 0.16	13.44 ± 0.11
System D: $z_{\text{abs}} = 2.5532$												
C IV λ 1548:												
1.....	5497.9	2.5512	-778	4.8 ± 0.7	0.37 ± 0.21	13.07 ± 0.35						
2.....	5500.1	2.5526	-896	11.0 ± 0.6	0.91 ± 0.35	13.15 ± 0.20	5500.1	2.5526	-896	9.5 ± 1.4	0.59 ± 0.34	13.34 ± 0.35
3.....	5500.9	2.5531	-939	13.1 ± 0.2	0.98 ± 0.01	14.28 ± 0.01	5501.0	2.5532	-947	14.4 ± 1.1	0.99 ± 0.03	14.17 ± 0.07
4.....	5501.5	2.5535	-972	8.1 ± 0.2	0.99 ± 0.00	15.05 ± 0.08	5501.5	2.5535	-972	8.9 ± 1.0	0.97 ± 0.02	14.82 ± 0.25

^a Parameters are obtained by a manual fitting method with C_f left as a free parameter. The uncertainties given here are the result of Poisson errors only and were evaluated by scanning parameter space, as discussed in § 4.1. The covering factors for components 1 and 3 (in the first spectrum) and 1 and 2 (in the second spectrum) were required to be the same.

^b Parameters are obtained by manual fitting, assuming $C_f = 1.0$. The uncertainties are discussed in § 4.1.

^c Parameters are obtained by automatic fitting, assuming $C_f = 1.0$. The errors quoted here reflect only the uncertainties due to Poisson noise.

TABLE 2
METAL LINES IN THE SECOND SPECTRUM

Line ID (1)	λ_{obs} (Å) (2)	z_{abs} (3)	V (km s ⁻¹) (4)	b (km s ⁻¹) (5)	C_f (6)	$\log N$ (cm ⁻²) (7)
System B: $z_{\text{abs}} = 2.4785$						
C II $\lambda 1335$:						
1.....	4639.4	2.4764	5608	4.8 ± 0.9	...	13.28 ± 0.06
2.....	4641.6	2.4781	5461	13.0 ± 1.4	...	14.04 ± 0.05
3.....	4642.2	2.4785	5427	10.4 ± 3.3	...	14.28 ± 0.13
4.....	4642.4	2.4787	5409	5.4 ± 1.8	...	13.87 ± 0.23
5.....	4642.8	2.4790	5383	17.8 ± 9.7	...	13.09 ± 0.17
6.....	4643.5	2.4795	5340	6.7 ± 2.1	...	12.97 ± 0.10
7.....	4643.8	2.4797	5323	6.0 ± 0.6	...	13.75 ± 0.06
8.....	4644.8	2.4805	5254	6.0 ± 0.6	...	13.96 ± 0.10
9.....	4645.8	2.4812	5194	4.0 ± 1.8	...	14.25 ± 0.66
10.....	4645.9	2.4813	5185	4.4 ± 1.5	...	13.76 ± 0.15
11.....	4646.3	2.4816	5159	5.6 ± 2.3	...	12.82 ± 0.12
N V $\lambda 1239$:						
1.....	4308.0	2.4775	5513	7.9 ± 1.3	0.70 ± 0.49	13.41 ± 0.49
2.....	4308.5	2.4779	5478	7.7 ± 4.3 ^a	...	12.48 ± 0.21 ^a
3.....	4308.9	2.4782	5452	13.5 ± 4.0 ^a	...	12.90 ± 0.11 ^a
4.....	4309.2	2.4785	5427	7.7 ± 1.1 ^a	...	12.69 ± 0.05 ^a
5.....	4309.5	2.4787	5409	^b	^b	^b
6.....	4309.9	2.4790	5383	9.0 ± 1.5 ^a	...	12.65 ± 0.12 ^a
O I $\lambda 1302$:						
1.....	4529.6	2.4785	5427	8.3 ± 0.3	...	14.34 ± 0.03
2.....	4533.1	2.4812	5194	12.2 ± 5.4	...	13.43 ± 0.15
Si II $\lambda 1260$:						
1.....	4381.4	2.4761	5634	4.6 ± 1.5	...	12.03 ± 0.08
2.....	4381.7	2.4764	5608	3.1 ± 0.7	...	12.49 ± 0.08
3.....	4383.6	2.4779	5478	3.2 ± 1.4	...	12.18 ± 0.11
4.....	4383.9	2.4781	5461	10.7 ± 1.2	...	13.04 ± 0.03
5.....	4384.4	2.4785	5427	2.6 ± 8.1	...	15.96 ± 0.49
6.....	4384.6	2.4787	5409	10.2 ± 3.6	...	12.90 ± 0.31
7.....	4385.5	2.4794	5349	6.4 ± 1.6	...	12.11 ± 0.08
8.....	4385.9	2.4797	5323	5.3 ± 0.5	...	12.82 ± 0.05
9.....	4386.9	2.4805	5254	5.4 ± 0.4	...	13.02 ± 0.06
10.....	4387.8	2.4812	5194	4.9 ± 0.7	...	13.09 ± 0.10
11.....	4388.0	2.4814	5177	3.2 ± 0.9	...	12.41 ± 0.07
Si III $\lambda 1207$:						
1.....	4194.9	2.4769	5564	28.4 ± 4.5	...	14.34 ± 0.38
2.....	4196.1	2.4779	5478	55.3 ± 35.3	...	13.79 ± 0.24
3.....	4196.9	2.4786	5418	8.8 ± 8.9	...	14.05 ± 2.42
4.....	4197.4	2.4790	5383	12.4 ± 5.2	...	12.75 ± 0.30
5.....	4198.0	2.4795	5340	7.3 ± 3.4	...	12.95 ± 0.28
6.....	4198.3	2.4797	5323	32.7 ± 6.0	...	13.10 ± 0.14
7.....	4198.3	2.4797	5323	2.6 ± 0.4	...	14.50 ± 0.68
8.....	4199.2	2.4805	5254	7.4 ± 1.2	...	13.24 ± 0.24
9.....	4200.1	2.4812	5194	4.1 ± 1.4	...	12.48 ± 0.11
10.....	4200.3	2.4814	5177	5.2 ± 1.9	...	12.34 ± 0.11
Si IV $\lambda 1394$:						
1.....	4845.1	2.4763	5616	12.7 ± 5.7	...	12.10 ± 0.34
2.....	4845.2	2.4764	5608	4.5 ± 0.5	...	13.10 ± 0.05
3.....	4846.8	2.4775	5513	6.6 ± 0.8	...	12.43 ± 0.04
4.....	4847.3	2.4779	5478	3.3 ± 0.6	...	12.66 ± 0.05
5.....	4847.8	2.4782	5452	20.6 ± 3.2	...	13.01 ± 0.05
6.....	4848.3	2.4786	5418	9.6 ± 0.8	...	13.08 ± 0.04
7.....	4848.9	2.4790	5383	14.4 ± 1.4	...	12.89 ± 0.03
8.....	4849.7	2.4796	5332	24.8 ± 2.3	...	12.99 ± 0.04
9.....	4850.0	2.4798	5314	4.6 ± 0.9	...	12.74 ± 0.07
10.....	4851.0	2.4805	5254	5.8 ± 0.5	...	13.17 ± 0.06
System D: $z_{\text{abs}} = 2.5532$						
Si IV $\lambda 1394$:						
1.....	4952.2	2.5531	-939	10.0 ± 1.1	0.77 ± 0.42	12.91 ± 0.30
2.....	4952.7	2.5535	-972	8.5 ± 0.4	0.94 ± 0.07	13.39 ± 0.07

TABLE 2—*Continued*

Line ID (1)	λ_{obs} (Å) (2)	z_{abs} (3)	V (km s ⁻¹) (4)	b (km s ⁻¹) (5)	C_f (6)	$\log N$ (cm ⁻²) (7)
System E: $z_{\text{abs}} = 1.8875$						
C IV $\lambda 1548$:						
1.....	4470.1	1.8873	60471	27.1 ± 2.9	0.95 ± 0.28	13.80 ± 0.17
2.....	4470.9	1.8878	60422	16.1 ± 3.2	0.50 ± 0.23	13.70 ± 0.30
System F: $z_{\text{abs}} = 1.9644$						
C IV $\lambda 1548$:						
1.....	4587.3	1.9630	52985	11.2 ± 2.3	0.47 ± 0.19	13.50 ± 0.26
2.....	4587.8	1.9633	52956	7.1 ± 0.7	0.96 ± 0.05	13.86 ± 0.07
3.....	4587.9	1.9634	52946	7.7 ± 0.5	0.98 ± 0.06	13.76 ± 0.06
4.....	4588.5	1.9638	52907	3.0 ± 2.6	0.11 ± 0.02	15.82 ± 3.57
5.....	4589.5	1.9644	52848	8.3 ± 0.5	0.96 ± 0.03	13.98 ± 0.06
6.....	4589.8	1.9646	52828	11.7 ± 3.3	0.69 ± 0.40	13.34 ± 0.33
7.....	4590.2	1.9649	52799	8.6 ± 1.1	0.76 ± 0.15	13.48 ± 0.13
8.....	4590.4	1.9650	52789	7.2 ± 1.5	0.73 ± 0.69	13.06 ± 0.51
System G: $z_{\text{abs}} = 2.0701$						
C IV $\lambda 1548$:						
1.....	4752.5	2.0697	42643	6.6 ± 1.1	1.29 ± 0.40	13.38 ± 0.23
2.....	4753.0	2.0700	42614	19.4 ± 1.8	1.04 ± 0.05	14.16 ± 0.05
Si IV $\lambda 1403$:						
1.....	4306.2	2.0698	42633	13.2 ± 2.5	...	13.10 ± 0.06
2.....	4306.6	2.0701	42604	6.8 ± 2.1	...	12.75 ± 0.11
System H: $z_{\text{abs}} = 2.2653$						
C IV $\lambda 1548$:						
1.....	5055.2	2.2652	24357	5.8 ± 1.8	0.49 ± 0.30	13.23 ± 0.33
2.....	5055.5	2.2654	24339	... ^c	... ^c	... ^c
Si III $\lambda 1207$:						
1.....	3939.5	2.2652	24357	3.6 ± 5.6	...	13.02 ± 2.41

^a Parameters are obtained by automatic fitting, assuming $C_f = 1.0$.

^b Component 5 could not be fitted for a continuum that gives a physical solution for the other components. N V $\lambda 1243$ could be contaminated by a blend or affected by correlated noise in this region.

^c It appears that component 2 of C IV $\lambda 1548$ is affected by a poor continuum fit or by contamination, since C IV $\lambda 1551$ is not detected at the same velocity, so no physical solution can be obtained.

To strengthen our results, we evaluate the covering factor using the following methods: (1) the “pixel-by-pixel” method—evaluating C_f for each pixel (using eq. [2]; e.g., Ganguly et al. 1999), and (2) the “automatic fitting” method—fitting absorption profiles using C_f , as well as $\log N$, b , and z_{abs} as free parameters in MINFIT (e.g., Ganguly et al. 2003). Unfortunately, neither method is applicable to system A because of heavy self-blending (i.e., blending of the *blue* members of some doublets with the *red* members of other doublets). Therefore, we adopt a third method for this system, *manual* fitting, which we apply only to components 1 and 2, where blending is not severe (see Figs. 2 and 3). In the manual fitting method we construct a simple model for the absorber with the same free parameters as in the MINFIT models. We then vary the free parameters over a wide range of values in small steps, assessing the goodness of the fit first by eye and then by the χ^2 test.

The C_f values with their 1σ “Poisson” errors, evaluated by the automatic fitting method, except for the C IV doublets in system A, are listed in Tables 1 and 2. The Poisson errors are uncertainties in the model parameters resulting from only Poisson noise in the spectra. There are additional sources of uncertainty, of course, which we discuss in detail below. In § 5 we present the spectra and discuss the properties of the eight C IV

systems to which we have applied our analysis. In the case of system A, we had to fit the profiles of components 1 and 2 manually. We estimated the Poisson uncertainties for components 1 and 2 by scanning a range of values about the best fit for all interesting parameters and looking for a significant increase in χ^2 (see Lampton et al. 1976). The uncertainties, which are included in Table 1, are negligible compared to uncertainties resulting from continuum placement errors or line blending, which we discuss further below. The ultimate reason for the small Poisson uncertainties in these two components is that the S/N is high and the lines are relatively broad, spanning many pixels.

Our derived C_f values are subject to a number of additional uncertainties. One such uncertainty results from line blending. If two or more components are blended together, a direct estimation of the C_f value by the pixel-by-pixel method (eq. [2]) is not reliable. On the other hand, the results from the automatic fitting method are still reliable, especially for strong doublets, as long as they are not affected by self-blending. To evaluate the systematic uncertainty in the latter method, we performed a line-deblending test in which we synthesized three artificial C IV doublets [$\log(N/\text{cm}^{-2}) = 13.5, 14.0, 14.5$; $b = 35$ km s⁻¹; $C_f = 0.5$] separated by 100 km s⁻¹ from each other, introduced them into an artificial spectrum with a S/N similar to what we obtain in

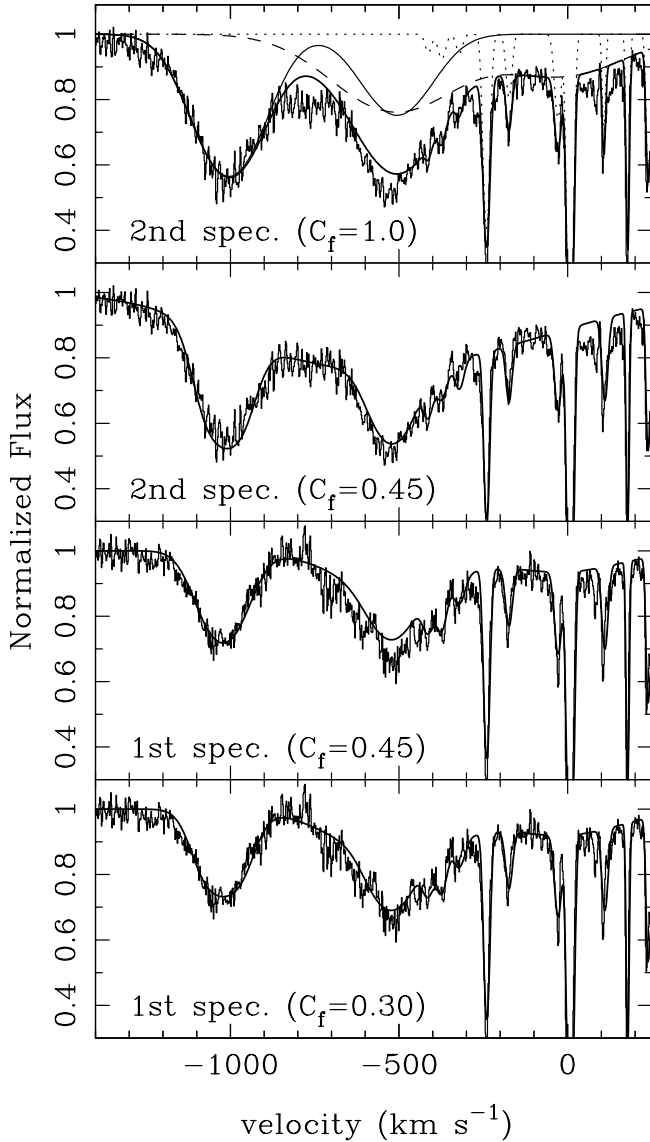


FIG. 2.—*Top*: Best-fitting model, with fixed $C_f = 1.0$, of the region around components 1 and 2 of system A in the second-epoch spectrum. Model profiles of each C IV doublet and Si II lines in system B are also plotted separately (light solid, dashed, and dotted lines, respectively). The final model is made to fit the blue member of the C IV doublet. The fit of the red doublet member is poor, illustrating that a model with full coverage is not acceptable. *Second panel*: Model that provides the best fit to the second-epoch spectrum with C_f treated as a free parameter. This fit is acceptable, yielding $C_f = 0.45$. *Third panel*: Model providing the best fit to the first-epoch spectrum with the covering factor fixed to $C_f = 0.45$, the value required by the second-epoch spectrum (all other parameters were left free). The model parameters were adjusted so as to fit the blue member of the C IV doublet. The fit to the red doublet member is poor, however, indicating that the covering factor must have varied between the two epochs. Additional details are given in § 4.1. *Bottom*: Model that provides the best fit to the first-epoch spectrum with C_f treated as a free parameter. This fit is acceptable, yielding $C_f = 0.3$.

practice, and determined their line parameters with MINFIT. We repeated this test 500 times. The distribution of resulting covering factors for the stronger lines is very narrow and centered very close to the input values; $C_f = 0.51 \pm 0.06$ and 0.51 ± 0.02 for doublets with $\log(N/\text{cm}^{-2}) = 14.0$ and 14.5 . However, the spread in the measured value of C_f is very large for weak doublets with $\log(N/\text{cm}^{-2}) = 13.5$. The outcome does not change significantly if we change the input C_f values. Thus, the result from the automatic fitting method is still reliable, at least for strong doublets with $\log(N/\text{cm}^{-2}) \geq 14.0$, even if there is line

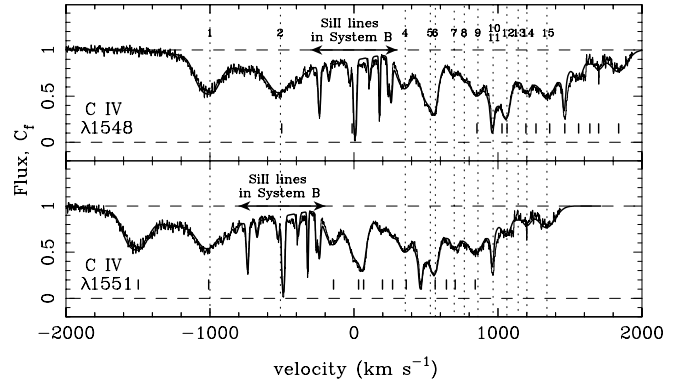


FIG. 3.—Velocity plots of the C IV doublets in system A at $z_{\text{abs}} = 2.4185 - 2.4455$ ($v_{\text{sh}} = 8300 - 10,600 \text{ km s}^{-1}$), detected in the second spectrum. Vertical dotted lines with ID numbers denote the positions of C IV doublets. Smooth lines are models fitted manually, using $C_f = 0.3$ for components 1 and 2, and $C_f = 1.0$ for the other components. The locations of the red and blue members of the 14 C IV doublets are also marked in the top and bottom panels to illustrate the severe blending.

blending (but not self-blending). However, one must still attach a systematic error of $\lesssim 10\%$ to C_f .

Continuum fitting also introduces an uncertainty in the derived values of C_f because it affects the residual flux in the absorbed spectral regions. We estimated an upper limit to the uncertainty in C_f resulting from continuum fitting errors through the following simulation: we shifted the normalized continuum level around the red member of the C IV doublet by the average noise level of the observed spectrum [$\sigma(f) \approx 0.015$] while keeping the continuum level around the blue doublet member fixed, and we investigated what the new value of C_f turns out to be, under the assumption that C_f was originally equal to 1. From this exercise we found that we obtain C_f values of 0.98, 0.93, 0.82, 0.56, and 0.13 (instead of 1) for normalized residual fluxes at the center of blue doublet members of 0.1, 0.3, 0.5, 0.7, and 0.9, respectively. Thus, we conclude that the C_f values for strong doublets (those with a normalized residual flux of ≤ 0.5) are uncertain by $\lesssim 20\%$. We regard this as an upper limit to the uncertainty because the effect of shifting the continuum on the value of C_f is smaller if (1) we perturb the continuum around both doublet members or (2) we assume that the original value of C_f is less than unity. In Table 3, we summarize upper and lower 1σ errors on C_f values in the case that C_f is less than unity. These were computed by shifting the continuum level only around the red member. Column (1) gives the C_f value, and columns (2)–(6) are the residual flux of the blue member of the doublet. We leave the entries blank for unphysical combinations of C_f and R_b . These tabulated values are the ones we adopt in our assessment of uncertainties.

We also considered the uncertainty resulting from the convolution of the spectrum with the line-spread function (LSF) of the spectrograph. This effect applies only to the pixel-by-pixel method (since automatic fitting convolves with the LSF) and was originally explored in the case of narrow doublets (widths comparable to the LSF width) by Ganguly et al. (1999). We performed the same analysis as Ganguly et al. but for broader doublets because most doublets in our sample are much broader than the LSF. We found that for isolated lines that are much broader than the LSF, the C_f values are evaluated correctly within a window around the line center whose width is twice the Gaussian broadening parameter ($2b$). This conclusion depends slightly on the line strength and width and is not valid if the doublet members are blended with each other (“self-blending”).

TABLE 3
ERROR BAR ON C_f FROM CONTINUUM FITTING UNCERTAINTY^a

C_f (1)	R_b^b				
	0.1 (2)	0.3 (3)	0.5 (4)	0.7 (5)	0.9 (6)
0.0.....
0.1.....	$<\pm 0.01$
0.2.....	+0.8
0.3.....	-0.09
0.4.....	$<\pm 0.01$	+0.7
0.5.....	+0.09	-0.18
0.6.....	-0.04	+0.6
0.7.....	+0.26	+0.5
0.8.....	-0.10	-0.37
0.9.....	+0.04	+0.4
1.0.....	-0.03	-0.47
0.0.....	...	$<\pm 0.01$...	+0.09	+0.3
0.1.....	...	+0.03	...	-0.06	-0.57
0.2.....	...	-0.02	...	+0.17	+0.2
0.3.....	...	+0.06	...	-0.10	-0.67
0.4.....	...	-0.04	...	+0.1	+0.1
0.5.....	...	+0	...	-0.14	-0.78
0.6.....	...	-0.02	...	+0	+0
0.7.....	...	-0.07	...	-0.18	-0.87

^a Blank entries indicate unphysical combinations of C_f and R_b .

^b R_b is the normalized residual intensity of the blue member of the doublet, relative to the *effective* continuum.

Outside this window, the C_f values are underestimated and can reach 0 in the far wings of the line. In these regions both the numerator and the denominator of equation (2) are very close to zero; therefore, the C_f values obtained with the pixel-by-pixel method are sensitive to the pixel width, the noise, and the sampling and interpolation schemes used in the calculation.

Considering all of the sources of error discussed above, the pixel-by-pixel method yields reliable results for our data in only very few cases. In the figures presented below, we plot the values of C_f from the pixel-by-pixel method only in the rare cases for which their uncertainties are reasonably small. Otherwise, we rely solely on the value of C_f derived by fitting the line profiles (either manually or using MINFIT).

4.2. Time Variability Analysis

The detection of time variability of absorption-line properties such as strengths, profiles, and shift velocities is another reliable method for identifying intrinsic NALs. Variability of absorption lines has been reported for a few Seyfert galaxies (e.g., Kraemer et al. 2002) and quasars (e.g., Gallagher et al. 2004; Hamann et al. 1997a). Recently, larger surveys looking for time-variable NALs have been carried out at $z \sim 2$ (Narayanan et al. 2004) and at $z \leq 1.5$ (Wise et al. 2004), and they detected variable NALs in 2 of 8 (25%) and 4 of 15 (27%) quasars, respectively. These fractions, however, are lower limits, since these studies used low- to medium-resolution spectra and are thus sensitive only to large variations.

To search for spectral variability in HS 1603+3820, we overplotted selected regions of the spectra from the two epochs and inspected them by eye (cf. Hamann et al. 1997a). This simple method is quite adequate because our spectra have a fairly high resolution and S/N, so even small changes are obvious to the eye. In summary, we found substantial variations in system A (Fig. 4) but not in any other absorption system (Fig. 5). We describe these changes along with other results in the following section. Possible causes of variability are (1) a change of ionization state and (2) a motion of the absorbing gas across the line of sight. We discuss these possibilities further in § 6.

5. RESULTS: NOTES ON EIGHT C IV SYSTEMS

We found 47 C IV, 14 Si IV, and six N V doublets, as well as another 54 single metal lines, such as Al II, Fe II, and Si II, be-

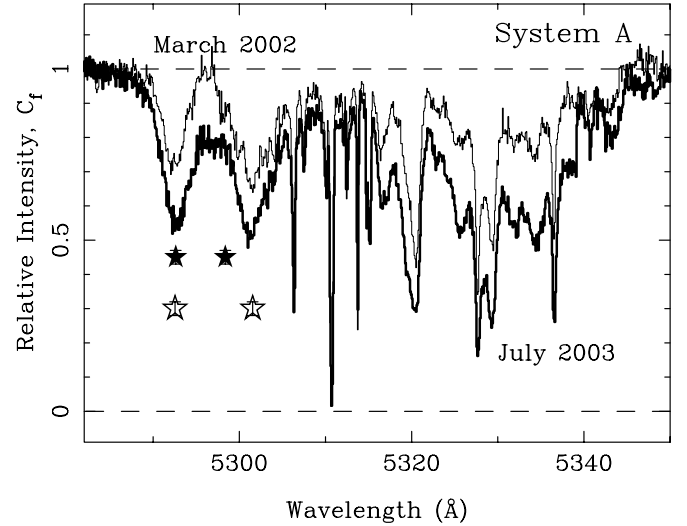


FIG. 4.—Normalized spectrum around C IV doublets in system A, in the first spectrum (*thin histogram*) and in the second spectrum (*thick histogram*). There is an obvious change in the absorption-line strength between the two epochs. Open and filled stars denote the covering factors for the first and second epoch, respectively (from manual fitting) with 1σ errors based on the uncertainty from the line blending only (see discussion of additional uncertainties in §§ 4.1 and 5; Poisson errors are negligible in comparison).

tween $z_{\text{abs}} = 1.88$ ($v_{\text{sh}} = 60,400 \text{ km s}^{-1}$) and $z_{\text{abs}} = 2.55$ ($v_{\text{sh}} = -950 \text{ km s}^{-1}$). For simplicity, we grouped the 121 components into eight absorption systems, which are discussed below. For the first four systems, which have already been discussed in M03, we performed both covering factor analysis and time variability analysis. For the other systems, we applied only covering factor analysis.

System A ($z_{\text{abs}} = 2.4185\text{--}2.4455$; $v_{\text{sh}} = 8300\text{--}10,600 \text{ km s}^{-1}$).—This system has many broad C IV doublets, and some of them are self-blended, which makes the line profile very difficult to decompose into kinematic components. In this case, the results from both the pixel-by-pixel and the automatic fitting methods are unreliable. Therefore, we concentrate on the wavelength region at $5290\text{--}5315 \text{ \AA}$, which can be decomposed relatively simply into two kinematic components of C IV plus several narrow Si II lines, and employ the manual fitting method described in § 4.1. If we assume full coverage, the best-fit model for the red (or blue) doublet member cannot reproduce the observed spectrum around the blue (or red) doublet member, as we illustrate in the top panel of Figure 2 using the second-epoch spectrum as an example. Thus, we resort to models with partial coverage, and we find coverage factors of 0.30 ± 0.02 and 0.45 ± 0.02 for the first- and second-epoch spectra, respectively (all sources of error included); i.e., we find a 5.3σ change in C_f . The uncertainties here are dominated by errors from line blending as estimated by the line-blending analysis in § 4.1; uncertainties due to continuum fitting (since $C_f = 0.5$ and $R_b \approx 0.5$; see Table 3) and Poisson noise are negligible in comparison (see § 4.1 and Table 1).

In the above analysis we assumed the same covering factors for the two components. We were led to make this assumption for the following reason: we first fitted the velocity region between -300 and $+250 \text{ km s}^{-1}$ with a broad C IV component only and found that the required covering factor was the same as that obtained for the narrow component after fitting a two-component (broad+narrow) model. After obtaining the best fit with the composite model we went back and relaxed the assumption that the two components had the same covering factors. We explored

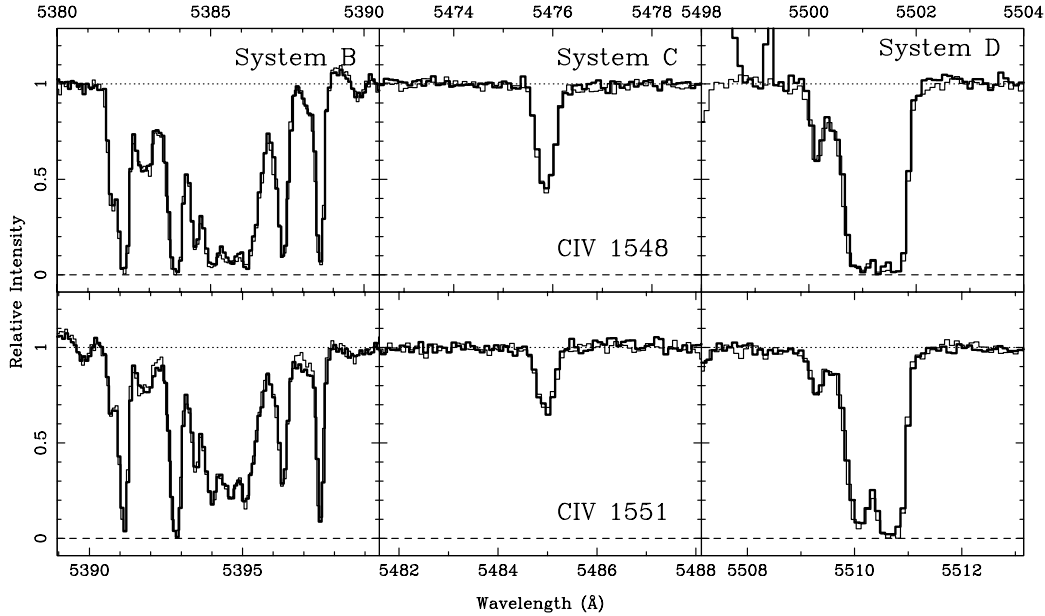


Fig. 5.—Same as Fig. 4, but for systems B, C, and D (binned by 10 pixels). The spectra from the two epochs are overplotted to illustrate the absence of variability in these three systems.

the consequences by perturbing the covering factors of the two components about the best fit and adjusting the column density to compensate. From this exercise we found that if the covering factors are not forced to be the same, they can deviate from the best fit by ± 0.015 in the first-epoch spectrum and by ± 0.03 in the second-epoch spectrum. If we treat these deviations as an additional error on C_f , we find that the change in C_f between the two epochs is 3.4σ , which is still fairly significant.

To illustrate the change in C_f we plot the observed line profiles from the two epochs in the second and third panels of Figure 2 with the best-fitting models for a fixed value of $C_f = 0.45$ superposed (all other parameters are free). It is clear from this figure that the first-epoch profile cannot be fitted adequately using the same value of C_f as the second-epoch profile. We also plot the best-fitting model to the first-epoch spectrum with $C_f = 0.3$ in the bottom panel.

In Figure 3 we present a fit to the entire system A, including the heavily blended region around 5315–5345 Å, for which we used the manual fitting method and assumed a fixed value of $C_f = 1$. The parameters obtained from this fit are listed in Table 1, although they should be regarded as tentative because of their large uncertainties. Deriving the uncertainties for these model parameters would have been extremely tedious and is not central to the point of this paper.

We identified 14 C iv doublets in this system, while D99 and M03 found five and seven doublets, respectively. Ly α , N v, and Si iv lines are also tentatively detected in our new spectrum. However, we cannot fit those profiles with MINFIT because they are very broad and strong. The continuum fits in these regions are not reliable. We cannot even apply the interpolation technique described in § 2 because echelle orders next to a given order are also affected by the Ly α forest.

For comparison of line profiles between the first and second spectra, we also superpose the two spectra in Figure 4. The strength of all doublets, including three narrow doublets, changes dramatically within 1.28 yr (0.36 yr in the quasar rest frame). We also found that both the shift velocity and the line width of the broad component has changed, while such a change was not noted for component 1. More specifically, the shift velocity of the

broad component changed by $\sim 210 \text{ km s}^{-1}$ (the uncertainty in the shift velocity is $\pm 5 \text{ km s}^{-1}$), while the b -parameter changed by $\sim 170 \text{ km s}^{-1}$ (the uncertainty in b is $\pm 8 \text{ km s}^{-1}$). Unfortunately, we cannot study these parameters for the other components because of heavy line blending. The Si II $\lambda 1527$ lines in system B at 5306–5314 Å do not change between the two observations, which suggests that our interpolation fitting method, described in § 2 and in M03, is effective. Although M03 suggested that the narrow C iv doublets could be independent of the other lines in system A based only on the result of the covering factor analysis, we find here that all 14 doublets change synchronously, and thus they are probably produced in the same intrinsic system. These C iv doublets show a sudden increase of their total equivalent width ($W_{\text{obs}} \approx 10.4 \rightarrow 19.1 \text{ \AA}$), which could mean that, in a later stage of evolution, many narrower components may blend with each other to make what resembles a BAL profile (Morris et al. 1986; Richards et al. 2002; M03). Weymann et al. (1991) defined BALs as systems with continuous absorption, spanning more than 2000 km s^{-1} , within which at least 10% of flux must be absorbed. The velocity width of system A, $\Delta v \sim 2300 \text{ km s}^{-1}$, satisfies this definition, although the normalized residual flux is more than 0.9 in some regions at the time of observation. Some examples of BALs are known to have different covering factors at different regions in the same system (Arav et al. 1999; Hutsemékers et al. 2004). BAL systems also sometimes have multiple components, which are analogous to the components of system A (Korista et al. 1993; Arav et al. 1999). These results support the hypothesis that the NAL cluster in system A could become a BAL, although additional observations will be necessary to confirm this. In § 6.3 we use simulations to illustrate the plausibility of the suggestion that this system could be evolving into a BAL.

System B ($z_{\text{abs}} = 2.4785$; $v_{\text{sh}} = 5400 \text{ km s}^{-1}$).—This strong C iv system consists of 15 narrow doublets with $b \leq 26 \text{ km s}^{-1}$. Some of them can be explained by pure thermal broadening (i.e., $b \leq 7.4 \text{ km s}^{-1}$ at $T_{\text{gas}} = 40,000 \text{ K}$). We present the velocity plots of 12 metal line transitions, including the C iv and N v doublets, in Figure 6. In cases that MINFIT gives unphysical C_f values (i.e., $C_f < 0$ or > 1), which happens for some components, probably because of heavy line blending, we assume

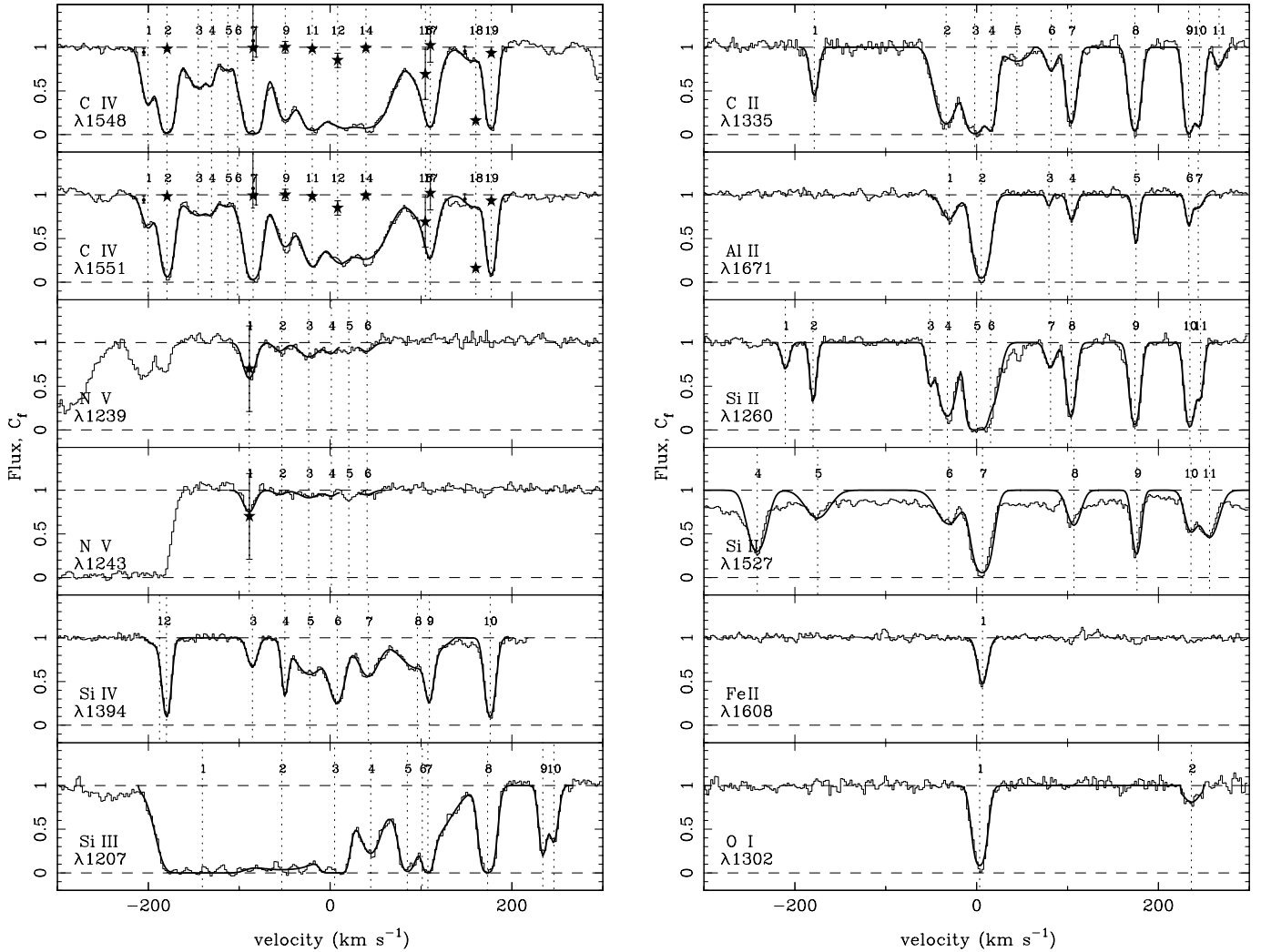


FIG. 6.—Velocity plots of various transitions in system B at $z_{\text{abs}} = 2.4785$ ($v_{\text{sh}} = 5400 \text{ km s}^{-1}$). Vertical dotted lines with ID numbers are positions of absorption lines. Smooth lines are model fits by MINFIT. Filled stars with error bars are covering factors determined by MINFIT. Small dots with error bars denote covering factors evaluated by the pixel-by-pixel method. In both cases, the error bars represent uncertainties from Poisson noise only; additional uncertainties are discussed in § 4.1.

$C_f = 1$ to estimate fit parameters. The covering factors of all doublets except for the component at $z_{\text{abs}} = 2.4804$ (ID 18) are consistent with full coverage as determined both by profile fitting and the pixel-by-pixel method. For the latter method, we do not plot C_f values if their error values are larger than 1.0. Component 18 of C IV $\lambda 1551$ is likely to be influenced by the unidentified blend apparent between components 17 and 18; thus, the low C_f measured for component 18 of C IV $\lambda 1551$ is discounted. Component 5 of N V $\lambda 1243$ may also be affected by a blend, since we were unable to obtain a physical solution in this region for any reasonable continuum fit.

System C ($z_{\text{abs}} = 2.5370$; $v_{\text{sh}} = 420 \text{ km s}^{-1}$).—This is one of two systems within 1000 km s^{-1} of the quasar. Besides the C IV doublet, there are no other metal lines detected in the second spectrum. We find neither partial coverage (Fig. 7) nor time variability (see Fig. 5) in spite of the very small velocity shift from the quasar.

System D ($z_{\text{abs}} = 2.5532$; $v_{\text{sh}} = -950 \text{ km s}^{-1}$).—This is another system within 1000 km s^{-1} of the quasar, but redshifted relative to the quasar. This system was resolved into four narrow doublets in M03. We are able to analyze only three doublets in the second spectrum because the bluest component of C IV $\lambda 1548$ is affected by a detector defect. Although Si IV, as well as C IV, is

identified in the system, neither shows partial coverage if we consider the error in the continuum fit (Fig. 8). The C_f value of C IV component 1 in the first spectrum is small, but the upper 1σ error would approach 1.0 once we consider continuum level error $\sigma(C_f) = 0.5$ from Table 3. We also do not find time variability of the C IV doublets (see Fig. 5). These results suggest that the

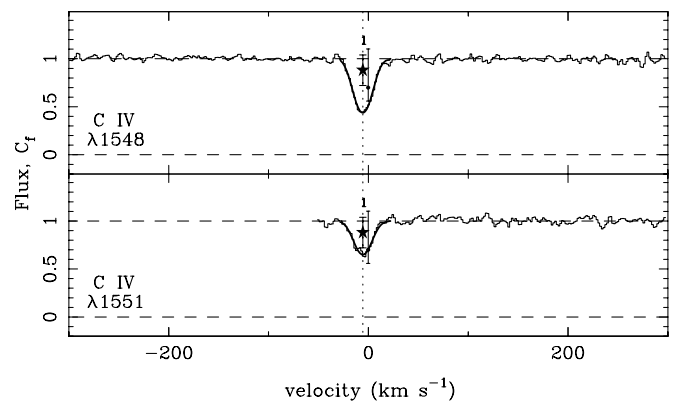


FIG. 7.—Same as Fig. 6, but for system C at $z_{\text{abs}} = 2.5370$ ($v_{\text{sh}} = 420 \text{ km s}^{-1}$).

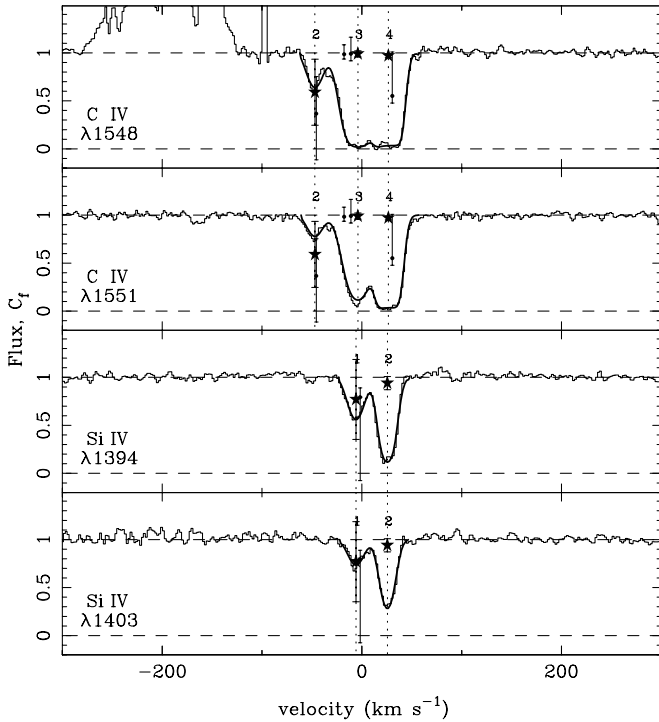


FIG. 8.—Same as Fig. 6, but for system D at $z_{\text{abs}} = 2.5532$ ($v_{\text{sh}} = -950 \text{ km s}^{-1}$).

absorber covers the background source entirely in the direction of this line of sight. Nevertheless, we still cannot rule out an intrinsic origin for systems C and D in the vicinity of the quasar (within 1000 km s^{-1}), especially because a number of intrinsic NALs have been detected at small velocities from quasars (e.g., Ganguly et al. 1999; Narayanan et al. 2004; Wise et al. 2004). We discuss these systems in § 6.

System E ($z_{\text{abs}} = 1.8875$; $v_{\text{sh}} = 60,400 \text{ km s}^{-1}$).—Two C iv doublets with line widths of $b = 16$ and 27 km s^{-1} are identified in the lowest redshift system in this study, which corresponds to $v_{\text{sh}} \sim 60,500 \text{ km s}^{-1}$ from the quasar (Fig. 9). One of the two doublets (component 2) has a small covering factor, $C_f = 0.5 \pm 0.2$, and the errors from continuum level uncertainty [$\sigma(C_f) = 0.1$] and line blending [$\sigma(C_f) \sim 0.06$] are also very small (in § 4.1). Despite its large shift velocity, this system could be classified as an intrinsic system. To confirm this possibility, additional evidence such as time variability is necessary.

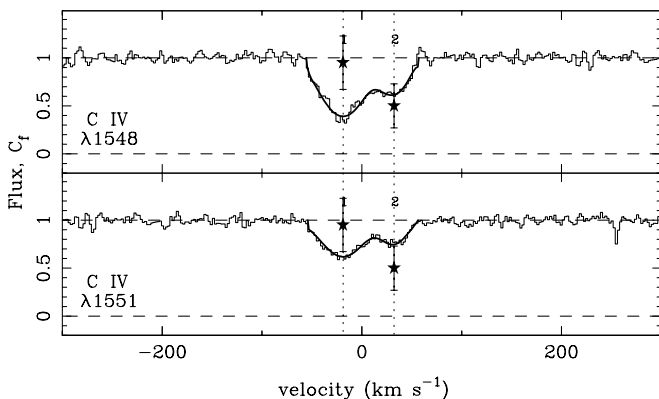


FIG. 9.—Same as Fig. 6, but for system E at $z_{\text{abs}} = 1.8875$ ($v_{\text{sh}} = 60,400 \text{ km s}^{-1}$).

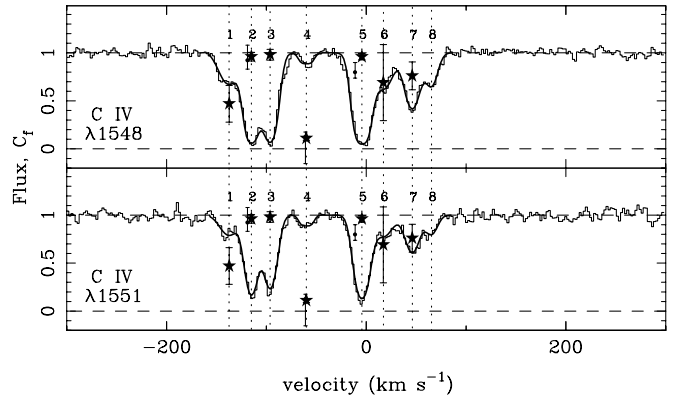


FIG. 10.—Same as Fig. 6, but for system F at $z_{\text{abs}} = 1.9644$ ($v_{\text{sh}} = 52,800 \text{ km s}^{-1}$).

System F ($z_{\text{abs}} = 1.9644$; $v_{\text{sh}} = 52,800 \text{ km s}^{-1}$).—Of eight C iv doublets in this system, five show full coverage (Fig. 10). The other three doublets (components 1, 4, and 7) have small C_f values. One of them (component 4) remains a candidate for an intrinsic doublet, even if we consider the error sources from both continuum level uncertainty [$\sigma(C_f) < 0.1$] and line blending [$\sigma(C_f) < 0.02$] (see discussion in § 4.1).

System G ($z_{\text{abs}} = 2.0701$; $v_{\text{sh}} = 42,600 \text{ km s}^{-1}$).—This system must also cover the quasar entirely because the line centers of the C iv $\lambda 1548$ transition are black (zero flux), which cannot happen in the case of partial coverage (Fig. 11). The covering factors of components 1 and 2 are consistent with unity. Corresponding Si iv absorption is apparently detected at $\Delta v = -30$ and 0 km s^{-1} (see Fig. 11), although the components at $\Delta v > 50 \text{ km s}^{-1}$ are N v doublets from system B. The components at $\Delta v \leq -50 \text{ km s}^{-1}$ for Si iv are also likely to arise from another system because no corresponding C iv doublets are detected. Unfortunately, we cannot evaluate the covering factor of the Si iv doublet because the Si iv $\lambda 1394$ line is blended with the Ly α forest.

System H ($z_{\text{abs}} = 2.2653$; $v_{\text{sh}} = 24,300 \text{ km s}^{-1}$).—A simple C iv system with two components, which was not detected in D99, is identified along with Si iii $\lambda 1207$ (see Fig. 12). The line

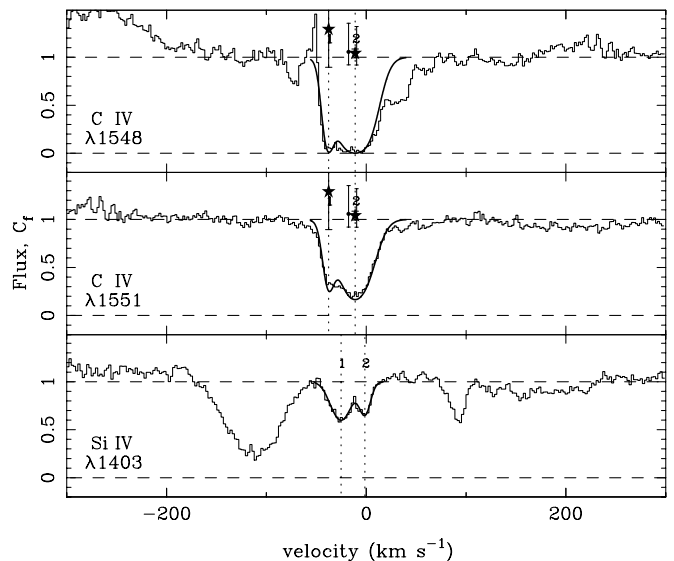


FIG. 11.—Same as Fig. 6, but for system G at $z_{\text{abs}} = 2.0701$ ($v_{\text{sh}} = 42,600 \text{ km s}^{-1}$).

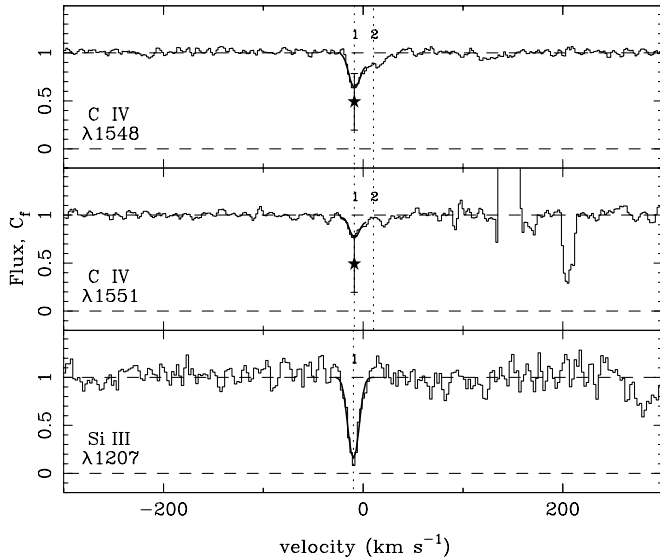


FIG. 12.—Same as Fig. 6, but for system H at $z_{\text{abs}} = 2.2653$ ($v_{\text{sh}} = 24,300 \text{ km s}^{-1}$).

center of Si III $\lambda 1207$ is well aligned with the C IV doublet. Although the covering factor determined by MINFIT is smaller than unity ($C_f = 0.5 \pm 0.3$) for component 1, we cannot rule out full coverage once we consider the uncertainties associated with setting the continuum level, $\sigma(C_f) = 0.2$, and with line blending (see discussion in § 4.1). This component, whose line width is comparable to the LSF, is affected by the convolution error. Therefore, the C_f values from the pixel-by-pixel method are not reliable. There is a large discrepancy between the model fit and the data in component 2 of the C IV $\lambda 1551$ line. This suggests that component 2 of the C IV $\lambda 1548$ line could have been misidentified as C IV or could be affected by continuum fitting uncertainty.

6. DISCUSSION: ORIGIN OF TIME VARIABILITY

Our main observational result is that system A shows a change of line strength within 0.36 yr in the quasar rest frame. No other system appears to be variable. The fact that system A is variable is compatible with the fact that it shows the signature of partial coverage and strengthens the case that the absorber is intrinsic to the quasar central engine.

There are at least two possible origins of time variability, (1) a change of the ionization state in the gas clouds and (2) motion of the absorbers across the line of sight to the background source(s). We discuss each of these possibilities below. Neither situation could arise if the absorbers are intervening clouds, unless they have high densities or sharp edges (Narayanan et al. 2004).

6.1. Change of the Ionization State

Supposing that the time variability is caused by a change in ionization state, we can place constraints on the electron density and the distance from the continuum source, following Hamann et al. (1997b) and Narayanan et al. (2004). These limits should be regarded with some caution because of the assumptions involved in obtaining them. We outline these assumptions below. Changes in the ionization state of the absorber can be caused by (1) a decrease in the ionizing flux causing recombination from the observed ionization state to the next lower state (C IV \rightarrow C III) or from the next higher state to the observed state (C V \rightarrow C IV) or (2) increase in the ionizing flux and subsequent photoionizations (C III \rightarrow C IV and C IV \rightarrow C V). Unfortunately, with

the available data we cannot assess whether the ionization state of the absorber of system A has changed or not. In order to do so we would have to resort to photoionization models, which would need to be constrained by absorption lines from a wide range of ionic species, which are not included in our spectra. Moreover, we cannot detect any changes in the observed continuum because the flux scale of our spectra is not calibrated. Therefore, we adopt the simplifying assumptions of Hamann et al. (1997b) and Narayanan et al. (2004), namely, (1) the gas is very close to ionization equilibrium, (2) changes in the ionizing flux are small, and (3) C IV is the dominant ionization state of C. Under these assumptions we can use the recombination timescale as a means of estimating the electron density (eq. [1] in Hamann et al. 1997b; eq. [1] in Narayanan et al. 2004; the recombination coefficient corresponds to a nominal gas temperature of 20,000 K, after Hamann et al. 1995). Using the rest-frame variability timescale ($t_{\text{var}} = 0.36 \text{ yr}$) as an upper limit to the recombination time, we estimate the minimum electron density to be $n_e \gtrsim 3 \times 10^4 \text{ cm}^{-3}$. We can also evaluate the maximum distance of the absorber from the continuum source by adopting the continuum shape of Narayanan et al. (2004) and using their equation (3) to connect the ionization parameter to the bolometric luminosity (the bolometric luminosity of HS 1603+3820, based on the prescription of Narayanan et al. [2004], is $L_{\text{bol}} = 2.5 \times 10^{48} \text{ ergs s}^{-1}$). Finally, we must also assume an ionization parameter of 0.02, which is the optimal value for C IV to be the dominant ionization state of C (Hamann et al. 1995, 1997a). This yields $r \lesssim 6 \text{ kpc}$. These limits on the electron density and the distance from the central source are very similar to the results for C IV and N V systems seen in the four quasars ($n_e \gtrsim 3400\text{--}40,000 \text{ cm}^{-3}$ and $r \leq 1.8\text{--}7 \text{ kpc}$) studied by Narayanan et al. (2004).

In conclusion, we note that regardless of changes in ionization state, however, we can conclude with reasonable confidence that the absorber is moving across the line of sight because the covering factor of the background source(s) is changing. In the next section we consider the implications of the variable covering factor in detail.

6.2. Motion of the Absorber

In the case of motion of the absorbers, the variability timescale could correspond to (1) the crossing time of clumpy gas across the background source or (2) the timescale on which the internal motion of the gas cloud changes the column density along the line of sight (e.g., Hamann et al. 1997a; Wise et al. 2004).

The variability timescale of system A is very short ($\sim 130 \text{ days}$), suggesting that the observed changes could not be produced by internal motions of the gas cloud, as we illustrate later in this section. Some intrinsic NALs detected in Narayanan et al. (2004) and Hamann et al. (1997a) also show very short variability timescales ($t_{\text{var}} = 0.28\text{--}0.40 \text{ yr}$) in the quasar rest frame. In these systems, the clumpy clouds could be moving across the line of sight to the continuum source. If this is the case for system A, we can derive some constraints on the size, crossing velocity, and distance of the absorber from the UV-emitting source using a simplified model as follows.

First, we assume that both the continuum source and broad-line region (BLR) are background sources (e.g., Ganguly et al. 1999). In this case, we can estimate the size of the BLR to be $R_{\text{BLR}} \sim 3 \text{ pc}$ by using the empirical relation between BLR size and the quasar luminosity that was found through reverberation mapping analysis (eq. [A3] in Vestergaard 2002). To apply this relation, we used the monochromatic continuum luminosity derived from the B magnitude of HS 1603+3820, measured by

D99. This luminosity is strictly an upper limit because at the redshift of the quasar the B filter includes a contribution from the Ly α and N v emission lines; nevertheless, the luminosity is overestimated only by a factor of a few.

Supposing that the absorbers have sharp edges, we estimate the crossing velocities as follows:

$$v_{\text{cross}} > [C_f(2) - C_f(1)] \frac{R_{\text{BLR}}}{t_{\text{var}}}, \quad (3)$$

where v_{cross} is the crossing velocity perpendicular to our line of sight (in the context of a disk wind model this is parallel to the surface of the accretion disk), $C_f(1)$ and $C_f(2)$ are covering factors in the first and second spectra, and t_{var} is the time interval between the two observations. Since t_{var} is really an upper limit to the variability timescale, equation (3) gives a lower limit to the crossing velocity. The crossing velocities of the two C iv components in system A (components 1 and 3 in the first spectrum or components 1 and 2 in the second spectrum), for which we can evaluate reliable C_f values in both spectra, would be $v_{\text{cross}} > 10^6 \text{ km s}^{-1}$. This model is implausible because the estimated speeds are much larger than the speed of light. Thus, we must conclude that the absorber covers primarily the UV continuum source and only a small part of the BLR. In fact, since the intensity of the broad C iv emission line at the location of system A is only about 10% of the continuum, the absorber giving rise to system A need not cover the BLR at all.

Therefore, we estimate the velocities by assuming that only the continuum source lies behind the absorbing clouds (e.g., Wise et al. 2004). We take $5R_S = 10GM_{\text{BH}}/c^2$ (where R_S and M_{BH} are the Schwarzschild radius and the mass of the black hole) as the continuum source size within which most of the UV continuum radiation is expected to originate. The central black hole mass is estimated by using an empirical relation that connects it to the UV luminosity and the width of the C iv emission line (eq. [8] in Vestergaard 2002). The UV luminosity was estimated as described above, and the FWHM of the C iv emission line (7500 km s^{-1}) was measured from the spectrum of D99. The resulting black hole mass is $4 \times 10^{10} M_{\odot}$, but we note that this value should be regarded with some caution because (1) the scatter about the empirical relation we have used can be as high as an order of magnitude and (2) the luminosity we have adopted is strictly an upper limit to the true value. Therefore, we believe that the black hole mass can be as low as a few $\times 10^9 M_{\odot}$. This model produces reasonable values of the crossing velocities, namely, $v_{\text{cross}} > 8000 \text{ km s}^{-1}$, using the higher black hole mass. We can also use the black hole mass to estimate an upper limit to the distance of the absorber from the background source, by requiring that the observed shift velocity does not exceed the escape velocity at that radius. From this consideration we obtain $r \lesssim 3 \text{ pc}$.

The above estimate of the crossing velocity can be used to argue against internal motions of the absorber as the origin of the change in the covering factor. Assuming that the speed of internal motions is comparable to the speed of sound, $c_s \approx 10T_4^{1/2} \text{ km s}^{-1}$ (where T_4 is the temperature in units of 10^4 K), the gas must be very hot to allow such fast internal motions. In particular, by setting $v_{\text{cross}} = c_s$ we obtain $T_{\text{gas}} \sim 6 \times 10^8 \text{ K}$, which is incompatible with the observed ionic species. We note, in conclusion, that using the size of the UV continuum source from the previous paragraph and the speed of sound for a 10^4 K gas, a typical variability timescale due to internal gas motions would be of the order of 100 yr.

We can derive more stringent, albeit more speculative, constraints on the location of the absorber if we adopt the dynamical model of Murray et al. (1995) for the radial and azimuthal motion of parcels of gas in an accretion disk wind. Following this model, we assume that the velocity of the gas in the radial direction follows $v_r(r) \simeq v_{\infty}(r_f)(1 - r_f/r)$, where r_f is the launch radius of a specific gas parcel and $v_{\infty}(r_f)$ is its terminal speed. Combining this with conservation of angular momentum and the expression for the terminal speed given in Chiang & Murray (1996) we obtain the following relation for the radius of the gas parcel relative to its launch radius:

$$\frac{r}{r_f} \approx 0.2 \left[\frac{v_r(r)}{v_{\varphi}(r)} \right] + 1, \quad (4)$$

where $v_{\varphi}(r)$ is the azimuthal speed of the parcel. To connect this expression to the observations, we identify the azimuthal velocity with the crossing velocity of the continuum source inferred from observations, i.e., $v_{\varphi}(r) = v_{\text{cross}}$. Moreover, we can take the velocity of system A to be the projection of the radial velocity along the line of sight, i.e., $v_r(r) \sin i = v_{\text{sys A}}$. If the inclination of the accretion disk is not very small ($\sin i > 0.2$), we can use equation (4) to obtain an upper limit on r/r_f . This limit will depend directly on the adopted mass of the black hole, since that determines the inferred crossing velocity. In view of the caveats associated with the estimated black hole mass, we choose to use the lowest plausible value, namely, $10^9 M_{\odot}$, which yields the most generous upper limit on the radius of the absorber, namely, $r/r_f \lesssim 10$. The launch radius of the wind is expected to be within the inner, radiation pressure-supported part of the accretion disk, which, for our inferred black hole mass and assuming an accretion rate close to the Eddington limit, is $5 \times 10^{16} \text{ cm}$ (Shakura & Sunyaev 1973; this is rather insensitive to the black hole mass). Thus, the constraint on the radius translates to $r \lesssim 0.2 \text{ pc}$. We also note the conclusion that $r/r_f < 10$ is in good agreement with the simulations of Proga et al. (2000), which show the wind fragmenting into filaments fairly close to its launch radius.⁷

6.3. Evolution to a BAL

The total equivalent width of system A has doubled within 0.36 yr in the quasar rest frame. This surprising growth is probably caused by (1) an increase of column densities and/or (2) an increase of the covering factors of the C iv doublets in the system, although the Doppler parameters could also be partially responsible. If the equivalent width continues to increase steadily, system A would satisfy all the requirements for a BAL classification.

In order to predict future profiles, we synthesize spectra by changing the column densities or the covering factors of the C iv doublets in the system. Unfortunately, we cannot evaluate the column density and covering factor of each doublet exactly in the observed spectrum, since the C iv doublets are heavily blended with each other or with Si II lines from system B. Therefore, we convert the column densities of the C iv doublets in the second spectrum in Table 1 (evaluated assuming $C_f = 0.45$ or 1.0) to values assuming $C_f = 0.7$ (corresponding to the depth of the deepest C iv component; we adopt this value for all components for simplicity) and use them below. We present simulated line profiles that are synthesized by multiplying the column densities by 0.5, 1.0, 2.0, and 5.0 (Fig. 13; here covering factors are fixed), or by changing the covering factors, $C_f = 0.3, 0.5, 0.7$, and 0.9

⁷ If we had chosen the higher black hole mass of $4 \times 10^{10} M_{\odot}$, we would have obtained $r/r_f \sim 1$ and $r \lesssim 0.02 \text{ pc}$.

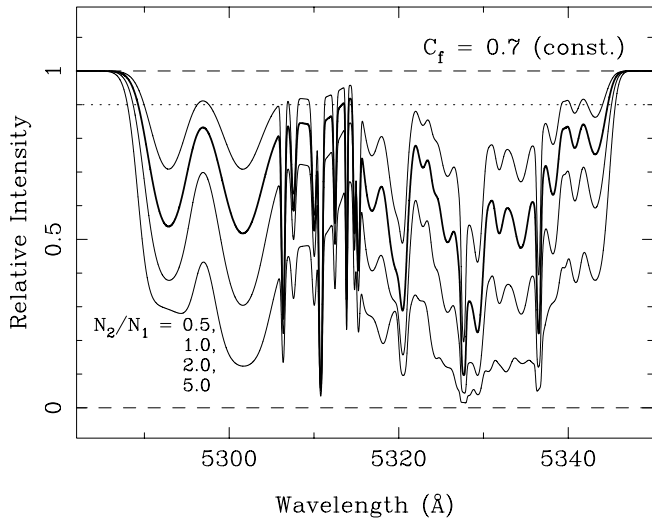


FIG. 13.—Model profiles of system A, synthesized by multiplying column densities of the C IV components by factors of $N_2/N_1 = 0.5, 1.0, 2.0,$ and 5.0 (top to bottom). The covering factors are assumed to be constant ($C_f = 0.7$ in all cases). The original column densities were estimated, assuming that $C_f = 0.7$ for all C IV doublets in the observed spectrum (except for the Si II lines in system B). The thick line corresponds to the original (observed) profile, while thin lines are model profiles for different column densities. The total velocity width of the system is about 2300 km s^{-1} . Therefore, the model profile is classified as a BAL if its normalized flux is weaker than 0.9 (horizontal dotted line) throughout the system. Two of the models ($N_2/N_1 = 2.0$ and 5.0) satisfy all the BAL criteria.

(Fig. 14; here column densities are fixed). Thick lines are the observed profiles, while thin lines are synthesized models. For three models (i.e., $N_2/N_1 = 2.0, 5.0,$ or $C_f = 0.9$), the continuum flux is absorbed by at least 10% over a velocity range of $>2000 \text{ km s}^{-1}$, which satisfies the definition of a BAL. If the Doppler parameters increase simultaneously, the blended C IV components make a smoother profile, whose appearance would be similar to those of BALs. With additional spectra taken at regular intervals, we could probe the origin of time variability further (i.e., distinguish between a change of column density and a change in covering factor) by comparing the observed line profiles with our simulations.

6.4. Physical States of Systems C and D

In systems C and D, we detect neither time variability nor partial coverage with our spectra taken over a 1.28 yr interval of observation, even though these would appear to be promising candidates for intrinsic systems because of their small shift velocities. There are at least three candidates for the origin of these systems. They can be produced in either (1) the quasar host galaxy, (2) intervening galaxies in the vicinity of the quasar that are members of the same cluster (or group) of galaxies, or (3) gas clouds intrinsically associated with the quasar that appear to be ejected (system C) or infalling (system D); these gas parcels can be part of a high-altitude stream in an accretion disk wind (which may be circulating) as simulated by Proga et al. (2000).

However, since we do not see the hallmarks of intrinsic absorption in either of these two systems (e.g., partial coverage or time variability), we cannot prove that they are intrinsic, nor can we rule this out. We find it unlikely that system D is made up of undisturbed gas in the host galaxy because of its large velocity shift. The fact that the absorption troughs in system D are black suggests that this absorber covers both the continuum source and the broad emission line region almost completely; i.e., its trans-

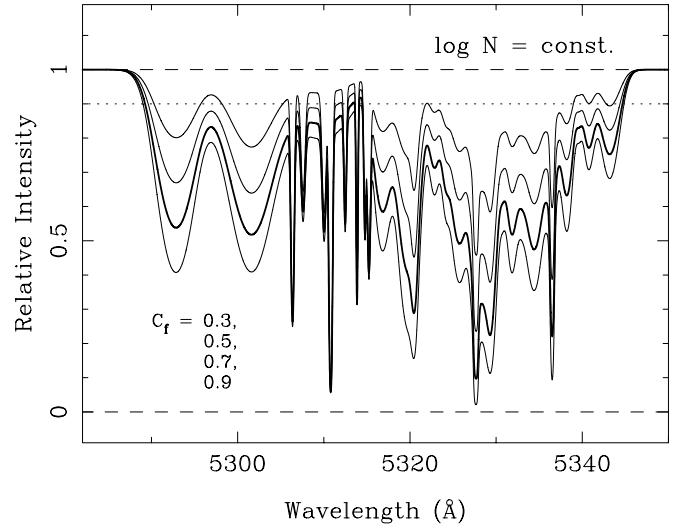


FIG. 14.—Same as Fig. 13, but synthesized by changing covering factors, $C_f = 0.3, 0.5, 0.7,$ and 0.9 (top to bottom). Column densities are fixed. One of these models ($C_f = 0.9$) satisfies the criteria for a BAL.

verse size could be a few parsecs (cf. § 6.2). This large size could also be responsible for the lack of variability, if this system is intrinsic.

6.5. Other Potentially Intrinsic Systems

Among the eight C IV systems, four (systems E–H) have been studied based on only covering factor analysis. In cases where the measured C_f value is small, the errors of C_f from continuum level uncertainty, as listed in Table 3, are small, and such components can be classified as intrinsic doublets: component 2 in system E ($C_f = 0.5 \pm 0.2$) and component 4 in system F [$C_f = 0.1$ with $\sigma(C_f)$ smaller than 0.1] (here errors from the line blending are negligible). These systems are potentially interesting because of their high velocities relative to the quasar: $v_{\text{sh}} \sim 60,400 \text{ km s}^{-1}$ (system E) and $52,800 \text{ km s}^{-1}$ (system F). Therefore, it is very important to monitor them further for time variability. We already know of several examples of high-velocity systems that are variable. These include the systems in Q0151+048 with $v_{\text{sh}} \sim 28,000 \text{ km s}^{-1}$, in PG 0935+417 with $v_{\text{sh}} \sim 52,000 \text{ km s}^{-1}$ (Narayanan et al. 2004), in Q2343+125 with $v_{\text{sh}} \sim 24,000 \text{ km s}^{-1}$ (Hamann et al. 1997a), and in PG 2302+029 with $v_{\text{sh}} \sim 56,000 \text{ km s}^{-1}$ (Jannuzi 2002).

7. CONCLUSIONS AND FUTURE WORK

We observed the quasar HS 1603+3820 for a second time with Subaru+HDS after an interval of 1.28 yr from the previous observation in order to perform time variability analysis for the C IV systems at $v_{\text{sh}} = -950$ – $10,600 \text{ km s}^{-1}$ from the quasar. We also applied covering factor analysis using two methods, the pixel-by-pixel method and Voigt profile fitting. Our main results are as follows:

1. Only system A ($v_{\text{sh}} \sim 8300$ – $10,600 \text{ km s}^{-1}$), which was identified as an intrinsic system by covering factor analysis in M03, shows strong time variability of the line strength and covering factor.
2. If a change of the ionization state causes the variability in system A, we can place constraints on the electron density ($n_e \gtrsim 3 \times 10^4 \text{ cm}^{-3}$) and the absorber's distance from the continuum source ($r < 6 \text{ kpc}$).

3. If gas motion across the background UV source causes the variability in system A, the crossing velocity and the distance from the continuum source are estimated to be $v_{\text{cross}} > 8000 \text{ km s}^{-1}$ and $r < 3 \text{ pc}$, respectively. In this case, the BLR cannot contribute significantly to the background UV flux (in fact, it need not contribute at all). If we adopt the dynamical model of Murray et al. (1995), we obtain an additional relation for the radius of the gas parcel relative to its launch radius, which gives a more strict, although model-dependent, constraint of $r < 0.2 \text{ pc}$.

4. We argue that the appearance of system A would be fairly similar to that of a BAL system if either the column densities of the C IV lines increase by factors of ≥ 2 or their covering factors become larger than 0.9.

5. Systems C and D ($v_{\text{sh}} \sim 420$ and -950 km s^{-1}) do not show any time variability, in spite of their small velocity distance from the quasar. They could still be intrinsic systems, but a more stringent test will have to await future observations.

6. Two systems (systems E and F; $v_{\text{sh}} = 60,400$ and $52,800 \text{ km s}^{-1}$) show suggestive evidence of an intrinsic origin based on only covering factor analysis. To confirm this, we would need other evidence for intrinsic NALs, such as time variability.

In order to investigate the nature of system C further, there are at least two possible future observations. If we observe this

quasar repeatedly at the appropriate time intervals (e.g., once a year), we may detect time variability in system C. This observation would have the additional benefit that we could detect the formation of a BAL in system A as we have speculated. Since the equivalent width of system A has doubled in only $\sim 1.3 \text{ yr}$, a few more observations may show dramatic evolution. We could also diagnose variations in the ionization state of the absorber by comparing observed spectra with our simulations. Spectropolarimetric observations would also be worthwhile because the degree of polarization in the troughs of intrinsic NALs could be much larger than those in intervening NALs, indicating scattering around the absorber. We believe that HS 1603+3820, one of the best laboratories for the investigation of intrinsic NALs, is an excellent target to monitor over a long period of time.

This work was supported by NASA grant NAG5-10817. We are grateful to the staff of the Subaru telescope, which is operated by the National Astronomical Observatory of Japan. We would also like to thank Christopher Churchill for providing us with the MINFIT software package, and Ben Lackey for his software to evaluate the pixel-by-pixel covering factors. Finally, we wish to thank the anonymous referee for many helpful comments and suggestions.

REFERENCES

- Arav, N., Becker, R. H., Laurent-Muehleisen, S. A., Gregg, M. D., White, R. L., Brotherton, M. S., & de Kool, M. 1999, *ApJ*, 524, 566
- Arav, N., Korista, K. T., Barlow, T. A., & Begelman, M. C. 1995, *Nature*, 376, 576
- Barlow, T. A., Junkkarinen, V. T., Burbidge, E. M., Weymann, R. J., Morris, S. L., & Korista, K. T. 1992, *ApJ*, 397, 81
- Barlow, T. A., & Sargent, W. L. W. 1997, *AJ*, 113, 136
- Carswell, R. F., Webb, J. K., Baldwin, J. A., & Atwood, B. 1987, *ApJ*, 319, 709
- Chiang, J., & Murray, N. 1996, *ApJ*, 466, 704
- Churchill, C. W. 1997, Ph.D. thesis, Univ. California, Santa Cruz
- Churchill, C. W., Vogt, S. S., & Charlton, J. C. 2003, *AJ*, 125, 98
- Crenshaw, D. M., Kraemer, S. B., Boggess, A., Maran, S. P., Mushotzky, R. F., & Wu, C.-C. 1999, *ApJ*, 516, 750
- Dobrzycki, A., Engels, D., & Hagen, H.-J. 1999, *A&A*, 349, L29 (D99)
- Dobrzycki, A., Engels, D., Hagen, H.-J., Elvis, M., Huchra, J., & Reimers, D. 1996, *BAAS*, 28, 829
- Foltz, C. B., Weymann, R. J., Peterson, B. M., Sun, L., Malkan, M. A., & Chaffee, F. H., Jr. 1986, *ApJ*, 307, 504
- Gallagher, S. C., Brandt, W. N., Wills, B. J., Charlton, J. C., Chartas, G., & Laor, A. 2004, *ApJ*, 603, 425
- Ganguly, R., Eracleous, M., Charlton, J. C., & Churchill, C. W. 1999, *AJ*, 117, 2594 (G99)
- Ganguly, R., Masiero, J., Charlton, J. C., & Sembach, K. R. 2003, *ApJ*, 598, 922
- Goodrich, R. W., & Miller, J. S. 1995, *ApJ*, 448, L73
- Hagen, H.-J., Groote, D., Engels, D., & Reimers, D. 1995, *A&AS*, 111, 195
- Hamann, F., Barlow, T. A., Beaver, E. A., Burbidge, E. M., Cohen, R., Junkkarinen, V., & Lynos, R. 1995, *ApJ*, 443, 606
- Hamann, F., Barlow, T. A., & Junkkarinen, V. 1997a, *ApJ*, 478, 87
- Hamann, F., Barlow, T. A., Junkkarinen, V., & Burbidge, E. M. 1997b, *ApJ*, 478, 80
- Hamann, F., & Sabra, B. 2004, in *ASP Conf. Ser. 311, AGN Physics with the Sloan Digital Sky Survey*, ed. G. T. Richards & P. B. Hall (San Francisco: ASP), 203
- Hutsemekers, D., Hall, P. B., & Brinkmann, J. 2004, *A&A*, 415, 77
- Jannuzi, B. 2002, in *ASP Conf. Ser. 254, Extragalactic Gas at Low Redshift*, ed. J. S. Mulchaey & J. T. Stocke (San Francisco: ASP), 13
- Korista, K. T., Voit, G. M., Morris, S. L., & Weymann, R. J. 1993, *ApJS*, 88, 357
- Kraemer, S. B., Crenshaw, D. M., George, I. M., Netzer, H., Turner, T. J., & Gabel, J. R. 2002, *ApJ*, 577, 98
- Lampton, M., Margon, B., & Bowyer, S. 1976, *ApJ*, 208, 177
- Misawa, T., Tytler, D., Iye, M., Storrie-Lombardi, L. J., Suzuki, N., & Wolfe, A. M. 2002, *AJ*, 123, 1847
- Misawa, T., Yamada, T., Takada-Hidai, M., Wang, Y., Kashikawa, N., Iye, M., & Tanaka, I. 2003, *AJ*, 125, 1336 (M03)
- Morris, S. L., Weymann, R. J., Foltz, C. B., Turnshek, D. A., Shectman, S., Price, C., & Boroson, T. A. 1986, *ApJ*, 310, 40
- Murray, N., & Chiang, J. 1995, *ApJ*, 454, L105
- Murray, N., Chiang, J., Grossman, S. A., & Voit, G. M. 1995, *ApJ*, 451, 498
- Narayanan, D., Hamann, F., Barlow, T., Burbidge, E. M., Cohen, R. D., Junkkarinen, V., & Lyons, R. 2004, *ApJ*, 601, 715
- Noguchi, K., et al. 2002, *PASJ*, 54, 855
- Proga, D., Stone, J. M., & Kallman, T. R. 2000, *ApJ*, 543, 686
- Richards, G. T. 2001, *ApJ*, 133, 53
- Richards, G. T., Gregg, M. D., Becker, R. H., & White, R. L. 2002, *ApJ*, 567, L13
- Richards, G. T., York, D. G., Yanny, B., Kollgaard, R. I., Laurent-Muehleisen, S. A., & Vanden Berk, D. E. 1999, *ApJ*, 513, 576
- Sargent, W. L. W., Boksenberg, A., & Steidel, C. C. 1988, *ApJS*, 68, 539
- Shakura, N. I., & Sunyaev, R. A. 1973, *A&A*, 24, 337
- Steidel, C. C. 1990, *ApJS*, 72, 1
- Vestergaard, M. 2002, *ApJ*, 571, 733
- Webb, J. K. 1987, Ph.D. thesis, Univ. Cambridge
- Weymann, R. J., Morris, S. L., Foltz, C. B., & Hewett, P. C. 1991, *ApJ*, 373, 23
- Wise, J. H., Eracleous, M., Charlton, J. C., & Ganguly, R. 2004, *ApJ*, 613, 129